

1 **The statistical emulators of GGCM phase 2: responses of year-to-year**
2 **variation of crop yield to CO₂, temperature, water and nitrogen**
3 **perturbations**

4
5 Weihang Liu^{1,2,3,4}, Tao Ye^{1,2,3,4*}, Christoph Müller⁵, Jonas Jägermeyr^{5,6,7}, James A.
6 Franke^{8,9}, Haynes Stephens^{8,9}, Shuo Chen^{1,2,3,4}

7
8 ¹ State Key Laboratory of Earth Surface Processes and Resource Ecology (ESPRE),
9 Beijing Normal University, Beijing, 100875, China

10 ² Key Laboratory of Environmental Change and Natural Disasters, Ministry of
11 Education, Beijing Normal University, Beijing 100875, China

12 ³ Academy of Disaster Reduction and Emergency Management, Ministry of
13 Emergency Management and Ministry of Education, Beijing 100875, China

14 ⁴ Faculty of Geographical Science, Beijing Normal University, Beijing 100875, China

15 ⁵ Potsdam Institute for Climate Impact Research (PIK), Member of the Leibniz
16 Association, Potsdam, Germany

17 ⁶ NASA Goddard Institute for Space Studies, New York City, New York, USA

18 ⁷ Center for Climate Systems Research, Columbia University, New York City, New
19 York, USA

20 ⁸ Department of the Geophysical Sciences, University of Chicago, Chicago, Illinois,
21 USA

22 ⁹ Center for Robust Decision- making on Climate and Energy Policy (RDCEP),
23 University of Chicago, Chicago, Illinois, USA

24
25

26 *** Corresponding author at:**

27 State Key Laboratory of Earth Surface Processes and Resource Ecology (ESPRE),
28 Beijing Normal University, 19 Xijiekouwai Street, Beijing, 100875, China.

29 E-mail: yetao@bnu.edu.cn

30

31 **Abstract**

32 Understanding the impact of climate change on year-to-year variation of crop yield is
33 critical to global food stability and security. While crop model emulators are believed
34 to be lightweight tools to replaces the raw models ~~per se~~, few emulators have been
35 developed to capture such interannual variation of crop yield in response to climate
36 variability. In this study, we developed a statistical emulator with machine learning
37 algorithm to reproduce the response of year-to-year variation of four crop yield to CO₂
38 (C), temperature (T), water (W) and nitrogen (N) perturbations defined in the Global
39 Gridded Crop Model Intercomparison Project (GGCMI) phase 2 experiment. The
40 emulators were able to explain more than 92.52% variance of simulated yield and
41 performed well in capturing the year-to-year variation of global average and gridded
42 crop yield over current croplands in the baseline. With the changes in CTWN
43 perturbations, the emulators could well reproduce the year-to-year variation of crop
44 yield over most current cropland. The variation of R and the mean absolute error was
45 small under the single CTWN perturbations and dual factor perturbations. These
46 emulators thus provide statistical response surfaces of yield, including both its mean
47 and interannual variability, to climate factors. They could facilitate spatiotemporal
48 downscaling of crop model simulation, projecting the changes in crop yield variability
49 in the future, and serving as a lightweight tool of multi-model ensemble simulation. The
50 emulators enhanced the flexibility of crop yield estimates and expanded the application
51 of large-ensemble simulation of crop yield under climate change.

52 **1. Introduction**

53 The impact of climate change on crop yield is an increasing concern of global food
54 security (Kinnunen et al., 2020). Two distinct approaches have been used to evaluate
55 the impact of climate change on crop yield, process-based crop models and statistical
56 models. Process-based crop models are reliable tools to project crop yields under future

57 climate change but computationally expensive (Jones et al., 2017). In contrast,
58 statistical models are lightweight tools that could fit yield response to historical climate
59 change (Li et al., 2019b) but the relationship between climate factors and crop yield is
60 limited by based on the current-historical climate conditions and their effects on crop
61 yields, which can hardly be used for future projection with new, unprecedented climate
62 conditions. Therefore, it is promising to develop tools that can reduce the expense of
63 computation and increase capacity for flexible future projections (Franke et al., 2020a).

64

65 Earlier studies have developed statistical emulators of process-based crop model results
66 to balance the advantages and disadvantages of process-based crop models and
67 statistical models. Those statistical emulators were initially developed with “entire
68 scenarios” (simultaneous changes in climate factors) simulation during historical or
69 future periods. Emulators have been developed for process-based crop models, like
70 APSIM (Shahhosseini et al., 2019), GEPIC (Folberth et al., 2019), GWG (Xu et al.,
71 2021), GAZE (Raimondo et al., 2021), and WOFOST (Tartarini et al., 2021), and used
72 to estimate historical crop yield. As the emulator trained by historical simulation could
73 not project the crop yield in the future, multiple crop model ensemble simulation in
74 future climate scenarios were used to calibrate emulators (Blanc, 2017, 2020; Blanc
75 and Sultan, 2015; Mistry et al., 2017; Ostberg et al., 2018). However, ~~t~~The scenario-
76 based future crop yield projection is not a systematic perturbation of climate factors
77 change (Franke et al., 2020a). For instance, the scenario-based yield projection can only
78 provide the simulated crop yield driven by simultaneous changes in climate factors. The
79 dependency of temperature and precipitation will be kept in scenarios, such that the
80 impact of temperature and precipitation cannot be clearly separated.

81

82 An alternative emulation based on “perturbated factors” training dataset was introduced,
83 which offers advantages to separate effects of crop yield drivers. The perturbated factors
84 emulation was first conducted on site-based crop model simulations, which could
85 estimate the yield across a broad range of CO₂, temperature and water (Fronzek et al.,

86 2018; Makowski et al., 2015; Pirttioja et al., 2015) but these emulators were limited to
87 the site-level. To break the constrain of site-based simulation, the global gridded crop
88 model intercomparison (GGCMI) phase 2 provided a simulation dataset across
89 structured CO₂-Temperature-Water-Nitrogen (CTWN) perturbation cubes. This dataset
90 offered two major advantages: it allows for separating the effects of different climatic
91 factors and of nitrogen levels on crop yields, and to distinguish the climatological-mean
92 and year-to-year variation of yields (Franke et al., 2020b). The phase 2 dataset was
93 published to support the derivation of crop yield- climate change “response surfaces”.
94 Based on the CTWN cubes, a statistical emulator has been developed providing near-
95 global-coverage multi-model emulators of climatological-mean yield projections from
96 the GGCMI Phase 2 ensemble by using a regression model with a third-order
97 polynomial basis function (Franke et al., 2020a). Due to the focus on climatological-
98 mean yield, the aspect of year-to-year variation of yield under CTWN perturbations has
99 not been fully analyzed or exploited in emulator design.

100

101 For climate change risk assessment, interannual yield variability (or the year-to-year
102 variation of yield) is an important metric of yield risk (Liu et al., 2021b) and food supply
103 stability (Liu et al., 2021a) but has been insufficiently addressed in previous studies
104 (Campbell et al., 2016). Large year-to-year variation of crop yield can influence
105 livelihoods of producers, food prices (Hasegawa et al., 2021), hunger (Janssens et al.,
106 2020) and even lead to political instabilities (Sternberg, 2011). Recently, year-to-year
107 variation has been introduced as a metric for climate change risk on global crop
108 production (Jägermeyr et al., 2021). Developing statistical emulators that can reproduce
109 the year-to-year variation of yield from the CTWN cubes could therefore provide a
110 powerful tool for studies focusing on the risk of climate change impact on yield. In this
111 study, we aimed exclusively to develop statistical emulators to reproduce year-to-year
112 yield variation with GGCMI phase 2 experiment data.

113 2. Data and Methods

114 2.1 Data

115 The input and output data for the simulation of global gridded crop yield were obtained
116 from the GGCM phase 2 experiment dataset, which includes gridded crop yield
117 projections at 0.5° longitudinal/latitudinal resolution for maize, spring wheat, winter
118 wheat, and rice, ~~and soybean~~ (Franke et al., 2020b). The input data for the process-
119 based simulations in GGCM Phase 2 included data of climate, soil, atmospheric CO₂
120 concentration, and nitrogen fertilizer application rates. Baseline (1980-2010) climate
121 inputs were used from the AgMIP Modern-Era Retrospective Analysis for Research and
122 Applications (AgMERRA) forcing dataset, including daily maximum and minimum
123 temperatures, precipitation, and solar radiation (Ruane et al., 2015). Systematic
124 perturbations were conducted in each grid cell with seven temperature levels (from -1
125 K to +6 K in 1K interval, with +5K skipped), nine precipitation levels (from -50% to
126 +30%, in 10% interval, with -40% skipped, the Winf precipitation level is simulation
127 under fully irrigated condition), four CO₂-concentration levels (360, 510, 660, and 810
128 ppm), and three nitrogen levels (10, 60, and 200 kg/ha). Simulations were repeated for
129 two adaptation strategies, i.e. no adaptation in cultivar (A0) and adaptation by
130 maintaining growing season length (A1). Twelve GGCMs were then forced with each
131 of these perturbations of the original reanalysis weather data. We selected 10 of 12 crop
132 models in the GGCM phase 2 experiment for constructing the emulators. These were
133 APSIM-UGOE, CARAIB, EPIC-IIASA, EPIC-TAMU, GEPIC, LPJ-GUESS, LPJmL,
134 ORCHIDEE-crop, pDSSAT, and PEPIC (Table1). PROMET and JULES were not
135 included as they used different climate inputs.

136

137 The GGCMs used a national and subnational crop calendar for crops that is based on
138 Sacks et al (2010), Portmann et al (2010), and environment-based extrapolations
139 (Elliott et al., 2015). The crop calendar was used to determine the window to calculate

140 the climatic predictors and grid-specific growing season length. The current global
 141 harvested area for identifying currently used cropland was obtained from the spatial
 142 production allocation model (SPAM) whose spatial resolution was 10km. The soil type
 143 data was obtained from the Harmonized World Soil Database (Nachtergaele et al.,
 144 2009).

145

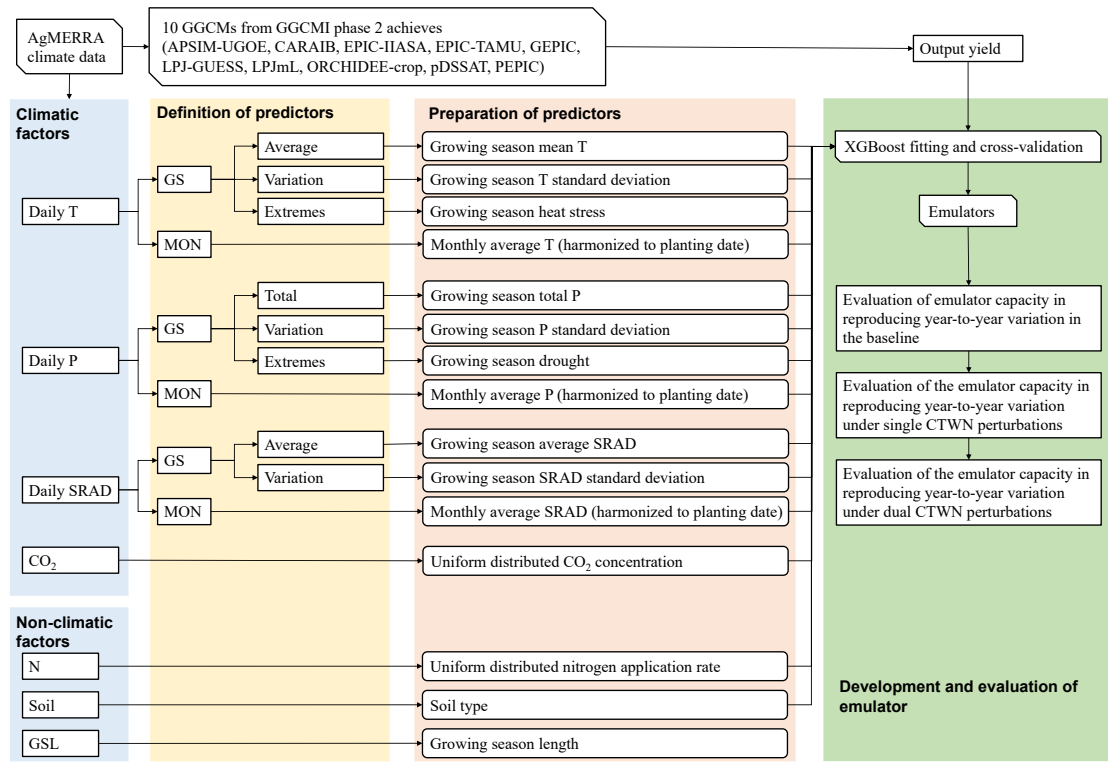
146 **Table 1** GGCMs included in emulation. Each model offers the same set of CTWN simulations across
 147 four crops.

GGCMs	Maize	Winter wheat	Spring wheat	Rice
APSIM-UGOE	√	√	√	√
CARAIB	√	√	√	√
EPIC-IIASA	√	√	√	√
EPIC-TAMU	√	√	√	√
GEPIC	√	√	√	√
LPJ-GUESS	×	√	√	×
LPJmL	√	√	√	√
ORCHIDEE-crop	√	√	×	√
pDSSAT	√	√	√	√
PEPIC	√	√	√	√

148 * LPJ-GUESS omits maize and rice, and ORCHIDEE-crop omits spring wheat (denoted by “×”)

149 2.2 Methods

150 Our study focused on the development and evaluation of emulators, which contains the
 151 following steps: 1) defining the predictors used to train the emulators; 2) preparing the
 152 predictors with climatic and non-climatic data; 3) training and cross validating the
 153 emulators with machine learning algorithm; and 4) evaluating the performance of
 154 emulators (**Figure1**).



155

156 **Figure 1** Overall framework of emulator development for GGCMs. Each GGCM-crop combination was
 157 calibrated as an emulator independently. T: temperature, processed separately for daily maximum, and
 158 minimum temperatures, P: precipitation, SRAD: solar radiation, N: nitrogen, Soil: soil properties. When
 159 developing irrigated yield emulator, the precipitation-related predictors are excluded.

160 **2.2.1 Definition and preparation of predictors**

161 All the predictors were computed or adapted from the GGCMs' input and output
 162 datasets. The climatic predictors were defined at two time-scales, growing season (GS)
 163 and monthly (MON) (**Table2**). The growing season average temperature, total
 164 precipitation and average solar radiation were able to explain the variation of
 165 climatological mean yield of GGCM phase2 (Franke et al., 2020a). To improve the
 166 capacity of emulators in reproducing the year-to-year variation of crop model yield,
 167 daily variability and extremes of climate factors during the growing seasons were
 168 considered here. The variation of temperature, precipitation and solar radiation during
 169 the growing seasons were calculated with the standard deviation of their daily values in
 170 each growing season, which represents the intensity of daily fluctuation of weather.
 171 Additionally, the heat and drought were selected to be the extreme climate predictors,
 172 which was quantified by extreme degree day (EDD, cumulative temperature that exceed

173 the high temperature threshold, Lobell et al., 2012) and maximum consecutive ~~drought~~
174 dry days (CDD, maximum length of consecutive days without precipitation, Troy et al.,
175 2015), because the negative effect of these two extremes could be shown by the current
176 GGCM (Heinicke et al., 2022). Other climate extremes, like excessive wetness, was not
177 used because the GGCM failed to show the negative effect (Li et al., 2019a; Liu et al.,
178 2022).

179

180 The monthly predictors only consisted of monthly average values. The monthly average
181 temperature, total precipitation and average solar radiation were harmonized according
182 to the specific planting date. The number of months was determined with the crop-
183 specific maximum growing season length over the global cropland defined by GGCM
184 phase2 experiment. For winter and spring wheat, we prepared the climatic predictors
185 over 10 and eight months after sowing. For maize and rice, climatic predictors over
186 eight and seven months after sowing were used, respectively.

187

188 The atmospheric CO₂ concentration and the nitrogen application rate were uniformly
189 distributed predictors. All years and grid cells were set at the same CO₂ concentration
190 and nitrogen application rate for each perturbation. Soil property is an important
191 temporally constant predictor, whose interaction with climate played important role in
192 yield simulation and emulator development (Blanc, 2017). As the soil parameter
193 settings of each GGCM varied, we selected the soil type at each grid to represent the
194 spatial variation of soil properties. There were 13 soil types, including heavy clay, silty
195 clay, light clay, silt clay loam, clay loam, silt, silt loam, sandy clay, loam, sandy clay
196 loam, sandy loam, loamy sand, sand. The most obvious difference across cultivars over
197 the global croplands is the growing degree requirement to reach maturity, which was
198 determined by both mean climatology and cultivar traits. To reproduce the length of
199 days from planting date to maturity date given by GGCM phase2 crop calendar
200 input~~spatial difference of simulated crop yield~~, we added a temporal constant growing
201 season length~~spatial difference term~~ as a predictor, i.e. temporal constant growing

202 season length.

203

204 As the purpose of emulator training is to develop a lightweight tool for crop simulation,
 205 there has always been a trade-off between the goodness-of-fit and the number of
 206 predictors. Therefore, we considered three strategies of using our predictors. “Strategy
 207 A” uses all predictors (the “Full” model), which is expected to derive the best goodness-
 208 of-fit. “Strategy B” uses only climatic predictors during growing season scale (the “GS”
 209 model), together with CO₂ concentration, nitrogen application rate and site information,
 210 soil class and growing season length. “Strategy C” uses only monthly average climatic
 211 predictors with other location-invariant predictors (the “Mon” model). In general,
 212 strategy B uses the smallest number of predictors, but those predictors need to be
 213 computed from daily climate forcing. Stagey C only relays on monthly climate data,
 214 and therefore is the least costly strategy for data preparation. A comparison between the
 215 three strategies would help us find a good balance between the predictors used and
 216 overall goodness-of-fit of the emulators.

217

218 **Table 2** Predictors of emulation. For rainfed yield emulators, we used all these predictors but for fully-
 219 irrigated yield emulators, the precipitation predictors were not included. Full, GS and Mon were three
 220 strategies to develop emulators. Full: developing emulators with all the climatic predictors; GS:
 221 developing emulators with climatic predictors during growing season scale; Mon: developing emulators
 222 with climatic predictors during monthly scale.

Predictor abbreviations	Descriptions	References	Full	GS	Mon	Time
Temperature related predictors						
GDD _{low-high_GS}	Growing degree day during growing season (winter wheat: low=0°C, high=30°C; spring wheat: low=5°C, high=30°C; maize: low=8°C, high=30°C; rice: low=10°C, high=35°C)	(Frieler et al., 2017; Jägermeyr et al., 2020; Lobell et al., 2012)				<u>1</u>
EDD _{high+_GS}	Extreme degree day during growing (winter and spring wheat, maize: high=30°C; rice: high=35°C)	(Lobell et al., 2012)				<u>1</u>
Tmax_GSmean	Average daily maximum temperature during growing season	(Zhu and Troy, 2018)				<u>1</u>

Tmin_GSmean	Average daily minimum temperature during growing season	(Zhu and Troy, 2018)	Blue	Green	White	1
Tmax_GSstd	Standard deviation of daily maximum temperature during growing season	(Zhu and Troy, 2018)	Blue	Green	White	1
Tmin_GSstd	Standard deviation of daily minimum temperature during growing season	(Zhu and Troy, 2018)	Blue	Green	White	1
Tmax_MONmean	Harmonized monthly average daily maximum temperature (MON=1–10 for winter wheat, MON=1–8 for spring wheat and maize, MON=1–7 for rice, since planting date)	(Folberth et al., 2019) (Jägermeyr et al., 2020)	Blue	White	Yellow	1
Tmin_MONmean	Harmonized monthly average daily minimum temperature (MON=1–10 for winter wheat, MON=1–8 for spring wheat and maize, MON=1–7 for rice, since planting date)	(Folberth et al., 2019) (Jägermeyr et al., 2020)	Blue	White	Yellow	1
Precipitation related predictors						
Pre_GSsum	Total daily precipitation during growing season	(Troy et al., 2015)	Blue	Green	White	1
Pre_GSstd	Standard deviation of daily precipitation during growing season	(Zhu and Troy, 2018)	Blue	Green	White	1
CDD_GS	Consecutive drought day (daily precipitation=0)	(Troy et al., 2015)	Blue	Green	White	1
Pre_MONsum	Harmonized monthly total precipitation (MON=1–10 for winter wheat, MON=1–8 for spring wheat and maize, MON=1–7 for rice, since planting date)	(Folberth et al., 2019) (Jägermeyr et al., 2020)	Blue	White	Yellow	1
Solar radiation related predictors						
SRAD_GSmean	Average daily solar radiation during growing season	(Folberth et al., 2019)	Blue	Green	White	1
SRAD_GSstd	Standard daily solar radiation during growing season	(Folberth et al., 2019)	Blue	Green	White	1
SRAD_MONmean	Harmonized monthly average daily solar radiation (MON=1–10 for winter wheat, MON=1–8 for spring wheat and maize, MON=1–7 for rice, since planting date)	(Folberth et al., 2019) (Jägermeyr et al., 2020)	Blue	White	Yellow	1
Greenhouse gas concentration						
CO ₂	CO ₂ concentration	(Franke et al., 2020a)	Blue	Green	Yellow	2
Non-climatic predictors						
N	Nitrogen fertilizer application	(Franke et al., 2020a)	Blue	Green	Yellow	2

Soil_type	Soil type	(Blanc, 2017)	
<u>SDTGSL</u>	Spatial difference term length	Growing_season (Folberth et al., 2019)	

223 *The colored the row denotes the predictors was included in the emulator. The column “Time” is defined
 224 to clarify the spatiotemporal dynamics of predictors: “1” represents both time and space variant
 225 predictors, “2” represents space invariant predictors, “3” represents time invariant predictors.

226 2.2.2 Emulator training and validation

227 Training the emulator of specific GGCM is to derive the response relationship between
 228 input and output, so that the emulator could replicate the complex process of yield
 229 simulation within the crop model. Emulation was trained by using machine learning
 230 regression on the GGCM-2 ensemble of crop- specific simulated yield with all CTWN
 231 perturbations. Each grid-year-perturbation combination was regarded as a sample in the
 232 fitting. We developed emulators of irrigated and rainfed yield and in A0 and A1
 233 scenarios separately. Since the outputs of GGCM outside the current croplands were
 234 not well examined, we trained the machine learning based emulators only on currently
 235 used cropland, according to the SPAM data for each crop separately.

236

237 The extreme gradient boosting (XGBoost) algorithm, a highly efficient realization of
 238 the gradient boosting approach that showed the best performance in recent machine
 239 learning challenges (Chen and Guestrin, 2016), was used to train the emulators. Key
 240 parameters in XGBoost, including the learning rate (0.1), the number of estimators
 241 (4000), and the maximum tree depths (10), were tuned by a grid search along parameter
 242 dimensions based on the default parameter as reference (Folberth et al., 2019). The
 243 goodness-of-fit of XGBoost was validated with the coefficient of determination R^2_{adjust} .

$$244 R^2_{adjust} = 1 - \frac{(n-1) \times (1 - R^2)}{n - k}$$

245 where n is the sample size of the validation set, k is the number of predictors.

246

247 Considering the spatiotemporal autocorrelation of simulated crop yield given by
 248 GGCM, we now used a “held out years and regions” strategy for leave one-year-out

249 cross-validation (Roberts et al., 2017; Sweet et al., 2023). Specifically, the all grid-year
250 samples are split into N folds. N is determined by the number of Köppen–Geiger (KG)
251 classes, which have more than 100 grid cells with harvested areas. If there are too few
252 harvested areas in one KG class, it will not be included in the cross-validation process.
253 For each fold of emulator training and validation, we withhold 10% of years (the last 3
254 years) and one entire KG class for validation, and the other grid-year samples are used
255 for training the emulator. We think selecting continuous years for validation can avoid
256 temporal autocorrelation. If we randomly select 10% of years, the correlation between
257 adjacent years still exist. Actually, any continuous three years are able to solve this
258 problem, such that we just use the last years according to the choice of (Sweet et al.,
259 2023).~~We used two validation strategies to show the goodness of fit. Firstly, we used a~~
260 ~~10-fold cross-validation that the samples were randomly divided into 10 folds, with~~
261 ~~nine of them used for training, and the rest used for validation. Secondly, considering~~
262 ~~the spatial autocorrelation in the raw GGCM simulated yield can invalidate the machine~~
263 ~~learning random selected validation sets (Ploton et al., 2020), we used the Köppen–~~
264 ~~Geiger climate regions to split the trained and validated sets. We used a leave-one-out~~
265 ~~approach that 29 out of the 30 climate regions were used for training, and the rest used~~
266 ~~for validation. The climate regions which contain less than 50 grids under current~~
267 ~~harvested areas will be removed from leave-one-out cross-validation process.~~
268 Emulators were trained in Python3.8 with GPU
269 (<https://xgboost.readthedocs.io/en/latest/python/index.html>).

270 **2.2.3 Evaluation of emulator**

271 Emulator performance was evaluated by comparing the 30-year emulated yield with the
272 30-year simulated yield of the GGCM. As we aimed at developing emulator that could
273 replicate the year-to-year variation of yield, the correlation coefficient (R), mean
274 absolute error (MAE) and mean relative error (MRE) were used to evaluate the
275 performance of emulators in the baseline and varied perturbations.

$$R = \frac{\sum_{i=1}^n (Y_{XGB,i} - \bar{Y}_{XGB})(Y_{GGCM,i} - \bar{Y}_{GGCM})}{\sqrt{\sum_{i=1}^n (Y_{XGB,i} - \bar{Y}_{XGB})^2 \cdot (Y_{GGCM,i} - \bar{Y}_{GGCM})^2}}$$

$$MAE = \frac{\sum_{i=1}^n |Y_{XGB,i} - Y_{GGCM,i}|}{n}$$

$$MRE = \frac{\sum_{i=1}^n |(Y_{XGB,i} - Y_{GGCM,i}) / Y_{GGCM,i}|}{n}$$

where n is the sample size of the validation set, $Y_{GGCM,i}$ is the annual simulated yield of the GGCMs, $Y_{XGB,i}$ is the annual projected yield of the XGB algorithm, and \bar{Y}_{XGB} and \bar{Y}_{GGCM} were the average XGBoost predicted and GGCM simulated yield, respectively.

3. Results

3.1 Goodness-of-fit of the emulators training

Overall, the emulator developed with XGBoost algorithm could well reproduce the variance of GGCM yield simulations, with adjusted R^2 greater than 0.920.52 (Table3). ~~The scatter plots of emulated yield and GGCM simulated yield for testing samples are clustered closely around the 1:1 ratio line (Figure S1).~~ For most emulators the adjusted R^2 under fully-irrigated (Winf) simulation were greater than those under rainfed simulation (W). Under A0 and A1 scenarios (The A0 denotes no adaptation and A1 denotes adaptation of the growing season to regain the original growing season length under warming scenarios that otherwise lead to accelerated phenology and thus shorter growing seasons.), the adjusted R^2 was comparable. For different crops, the performance of emulators developed for winter and spring wheat were slightly better than those developed for maize and rice. Among the GGCMs, ~~EPIC-HASAPEPIC~~'s behavior can best be emulated by emulators, with greatest R^2 values for all crops and scenarios. There are also several GGCM that is bit challenging for the XGB algorithm

to capture, i.e. winter wheat and ~~spring wheat~~rice simulation from ~~GEPIC~~~~ORCHIDEE-~~
~~crop~~, maize of pDSSAT, and ~~ricespring wheat~~ of ~~EPIC-TAMU~~~~LPJmL~~, with R^2 values
ranging from ~~0.920.52~~ to ~~0.960.63~~. When using the Köppen–Geiger climate regions to
~~apply the leave-one-out cross validation, the adjusted R^2 is generally smaller than those~~
~~obtained by the 10-fold cross validation with randomly selected samples, ranging~~
~~between 0.93 and 0.64 (Table S1).~~

Table 3 Adjusted R^2 of XGBoost derived from 10-fold cross validation with randomly selected samples

GGCMs (A0)	Winter wheat		Spring wheat		Maize		Rice	
	Winf	W	Winf	W	Winf	W	Winf	W
APSIM UGOE	0.99	0.97	0.98	0.97	0.92	0.94	0.96	0.96
CARAIB	0.98	0.98	0.98	0.98	0.97	0.97	0.98	0.97
EPIC IIASA	0.99	0.98	0.99	0.99	0.99	0.98	0.99	0.98
EPIC TAMU	0.97	0.97	0.97	0.97	0.94	0.97	0.93	0.97
GEPIC	0.97	0.95	0.98	0.96	0.97	0.95	0.97	0.96
LPJ-GUESS	0.99	0.98	0.99	0.98	-	-	-	-
LPJmL	0.98	0.98	0.98	0.98	0.94	0.96	0.95	0.96
ORCHIDEE-crop	0.99	0.98	-	-	0.98	0.96	0.97	0.97
pDSSAT	0.97	0.97	0.99	0.98	0.92	0.92	0.95	0.96
PEPIC	0.98	0.97	0.98	0.98	0.98	0.97	0.97	0.97

GGCMs (A1)	Winter wheat		Spring wheat		Maize		Rice	
	Winf	W	Winf	W	Winf	W	Winf	W
APSIM UGOE	0.99	0.96	0.98	0.96	0.96	0.92	0.97	0.96
CARAIB	0.98	0.98	0.99	0.99	0.97	0.97	0.98	0.97
EPIC IIASA	-	-	-	-	-	-	-	-
EPIC TAMU	0.98	0.98	0.97	0.97	0.95	0.97	0.94	0.97
GEPIC	0.98	0.96	0.98	0.97	0.98	0.97	0.98	0.97
LPJ-GUESS	0.99	0.99	0.99	0.99	-	-	-	-
LPJmL	0.98	0.99	0.97	0.98	0.94	0.96	-0.97	-0.96
ORCHIDEE-crop	-	-	-	-	-	-	-	-
pDSSAT	0.97	0.97	0.98	0.98	0.93	0.92	-0.96	-0.96
PEPIC	0.98	0.97	0.99	0.98	0.98	0.97	-0.97	-0.97

Table 3 Adjusted R^2 of XGBoost derived from 10-fold cross validation with randomly selected samples

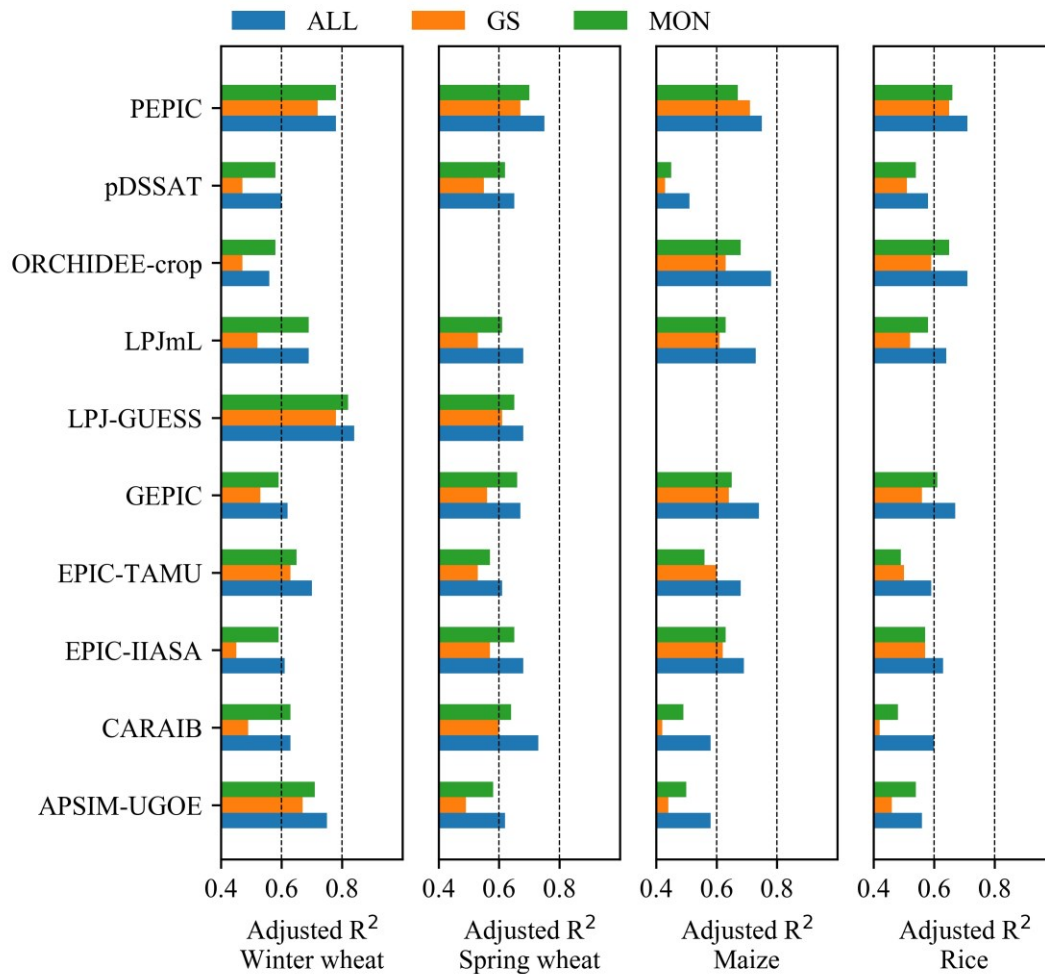
GGCMs (A0)	Winter wheat		Spring wheat		Maize		Rice	
	Winf	W	Winf	W	Winf	W	Winf	W
APSIM-UGOE	0.87	0.75	0.67	0.62	0.60	0.58	0.65	0.56
CARAIB	0.63	0.63	0.73	0.73	0.69	0.58	0.61	0.60

<u>EPIC-IIASA</u>	<u>0.68</u>	<u>0.61</u>	<u>0.70</u>	<u>0.68</u>	<u>0.67</u>	<u>0.69</u>	<u>0.71</u>	<u>0.63</u>
<u>EPIC-TAMU</u>	<u>0.65</u>	<u>0.70</u>	<u>0.80</u>	<u>0.61</u>	<u>0.77</u>	<u>0.68</u>	<u>0.67</u>	<u>0.59</u>
<u>GEPIIC</u>	<u>0.83</u>	<u>0.62</u>	<u>0.77</u>	<u>0.67</u>	<u>0.84</u>	<u>0.74</u>	<u>0.79</u>	<u>0.67</u>
<u>LPJ-GUESS</u>	<u>0.84</u>	<u>0.84</u>	<u>0.81</u>	<u>0.68</u>	=	=	=	=
<u>LPJmL</u>	<u>0.63</u>	<u>0.69</u>	<u>0.59</u>	<u>0.68</u>	<u>0.65</u>	<u>0.73</u>	<u>0.65</u>	<u>0.64</u>
<u>ORCHIDEE-crop</u>	<u>0.59</u>	<u>0.56</u>	=	=	<u>0.62</u>	<u>0.78</u>	<u>0.52</u>	<u>0.71</u>
<u>pDSSAT</u>	<u>0.63</u>	<u>0.60</u>	<u>0.69</u>	<u>0.65</u>	<u>0.55</u>	<u>0.51</u>	<u>0.63</u>	<u>0.58</u>
<u>PEPIC</u>	<u>0.80</u>	<u>0.78</u>	<u>0.90</u>	<u>0.75</u>	<u>0.85</u>	<u>0.75</u>	<u>0.79</u>	<u>0.71</u>
<u>GGCMs (A1)</u>	<u>Winter wheat</u>		<u>Spring wheat</u>		<u>Maize</u>		<u>Rice</u>	
	<u>Winf</u>	<u>W</u>	<u>Winf</u>	<u>W</u>	<u>Winf</u>	<u>W</u>	<u>Winf</u>	<u>W</u>
<u>APSIM-UGOE</u>	<u>0.85</u>	<u>0.73</u>	<u>0.69</u>	<u>0.64</u>	<u>0.60</u>	<u>0.59</u>	<u>0.62</u>	<u>0.56</u>
<u>CARAIB</u>	<u>0.59</u>	<u>0.58</u>	<u>0.73</u>	<u>0.71</u>	<u>0.64</u>	<u>0.53</u>	<u>0.71</u>	<u>0.68</u>
<u>EPIC-IIASA</u>	=	=	=	=	=	=	=	=
<u>EPIC-TAMU</u>	<u>0.67</u>	<u>0.61</u>	<u>0.76</u>	<u>0.64</u>	<u>0.81</u>	<u>0.63</u>	<u>0.68</u>	<u>0.60</u>
<u>GEPIIC</u>	<u>0.91</u>	<u>0.69</u>	<u>0.83</u>	<u>0.71</u>	<u>0.88</u>	<u>0.79</u>	<u>0.90</u>	<u>0.87</u>
<u>LPJ-GUESS</u>	<u>0.94</u>	<u>0.87</u>	<u>0.87</u>	<u>0.72</u>	=	=	=	=
<u>LPJmL</u>	<u>0.69</u>	<u>0.71</u>	<u>0.57</u>	<u>0.68</u>	<u>0.71</u>	<u>0.79</u>	<u>0.61</u>	<u>0.60</u>
<u>ORCHIDEE-crop</u>	=	=	=	=	=	=	=	=
<u>pDSSAT</u>	<u>0.67</u>	<u>0.64</u>	<u>0.75</u>	<u>0.69</u>	<u>0.63</u>	<u>0.58</u>	<u>0.69</u>	<u>0.63</u>
<u>PEPIC</u>	<u>0.80</u>	<u>0.76</u>	<u>0.90</u>	<u>0.75</u>	<u>0.88</u>	<u>0.77</u>	<u>0.86</u>	<u>0.77</u>

308 “-”: No GGCM simulation; Winf: irrigated condition; W: rainfed condition. The A0 denotes no
309 adaptation and A1 denotes cultivar adaptation to regain original growing season length under warming
310 scenarios.

311
312

313 The adjusted R^2 of emulators developed with all predictors (“Full model”) was greater
314 than those developed with growing season predictors (“GS model”) and monthly
315 predictors (“MON model”) (**Figure 2**). ~~If we validated using the 10-fold randomly~~
316 ~~selected sample approach, the performances of “GS model” and “MON model” were~~
317 ~~good and comparable to the “Full Model”. Nevertheless, the difference in performance~~
318 ~~became much pronounced when validated by using the climate-zone based leave-one-~~
319 ~~out approach (Figure S2).~~ GS models would suffer from reduced number of predictors
320 and their adjusted R^2 s were 0.1~0.15 smaller than corresponding MON models. Still,
321 Full models had the largest adjusted R^2 at the cost of the largest number of predictors.
322 For later usage of the emulators, a trade-off must be taken between cost of preparing
323 predictors and model goodness-of-fit, and the “MON model” could be a balanced
324 choice as it required only monthly average weather conditions.



325

326 **Figure 2** Adjusted R^2 of emulators (10-fold cross validation with randomly selected samples) with
 327 different strategy of predictors. All: “Full model”, GS: “GS model”, MON: “MON-Mon model”.
 328 Emulators for ORCHIDEE by spring wheat, and LPJ-GUESS by Maize and Rice were not fitted due to
 329 the lack of simulation of raw GGCM.

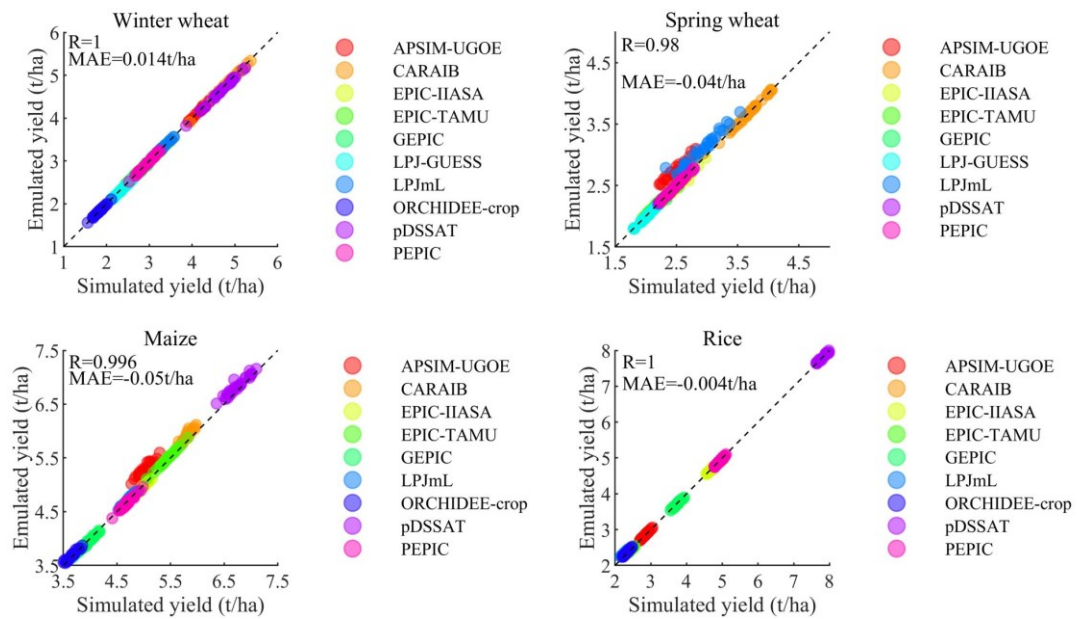
330 3.2 Performance of emulators to capture the year-to-year variation of GGCM

331 yield in the baseline

332 3.2.1 Performance of individual emulators at the global scale

333 Over current global cropland, the emulator of each GGCM could well reproduce the
 334 year-to-year variation of global average yield in the baseline period (during 1981–2010)
 335 (**Figure 3**). All individual emulators could capture the corresponding GGCM simulated
 336 yield, with scatters concentrated in the 1:1 ratio line. Different GGCM simulated yield
 337 levels varied from 1.7 to 7.8 t/ha but the performance of emulators has not been

338 influenced.



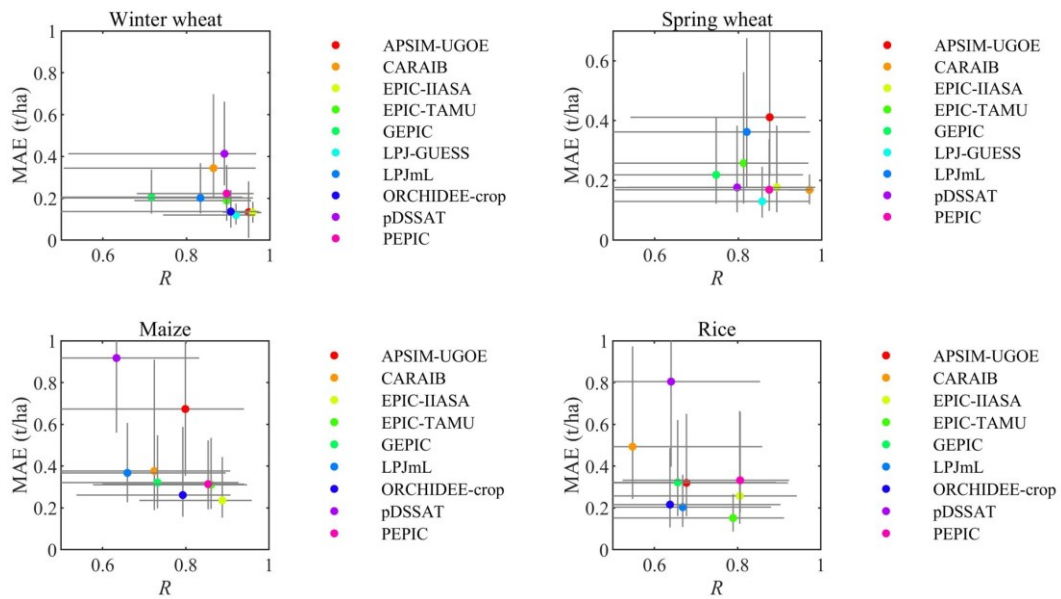
339

340 **Figure 3** Emulator performance to reproduce the year-to-year variation of global average yield (1981 –
341 2010) over current cropland. As ORCHIDEE-crop has not simulated yield under C360T0W0N200, we
342 used the C360T0W10N200 as the baseline. Each point with the same color is yield in 30 year. R is
343 correlation coefficient and MAE is mean absolute error.

344 3.2.2 Performance of individual emulators at grid scale

345 The overall performances of emulators at grid level were good for most crop-GGCM
346 combinations in the baseline. The performance of each emulator over current global
347 cropland grids were plotted by using scatter of MAE and R (**Figure 4**). The capacity of
348 emulators in reproducing the wheat yield simulated by GGCMs was better than that of
349 maize and rice. The median R over current winter and spring wheat harvested areas
350 were greater than 0.90.7. The R of the EPIC-TAMU-emulator and the LPJ-GUESS-
351 emulator were relatively smaller than other eight emulators developed for winter and
352 spring wheat, respectively. The median MAEs over current winter and spring wheat
353 harvested areas were less than 0.4 t/ha and 0.3 t/ha for winter and spring wheat
354 emulators, respectively, and the MAEs of the pDSSAT-emulator and LPJmL-emulator
355 were relatively greater. Over current maize harvested areas, the median R was greater
356 than 0.850.6 and the median of MAE was less than 0.40.7 t/ha, except pDSSAT-
357 emulator. The median R of emulators developed for rice were greater than 0.890.5, and

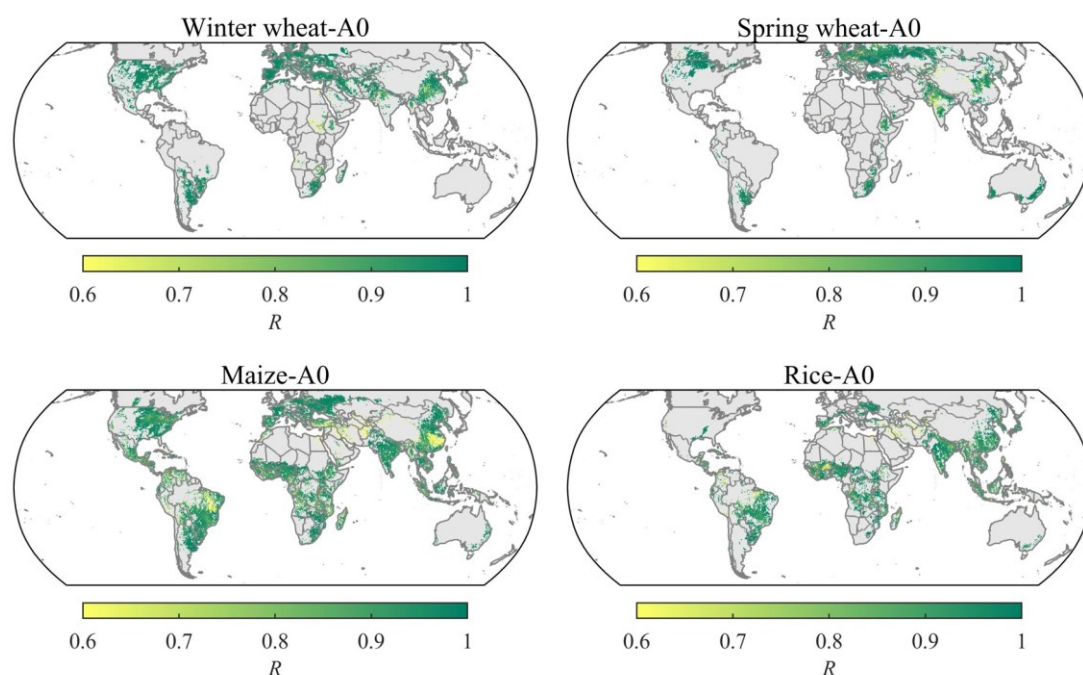
358 the median MAE were less than 0.30.4 t/ha over current rice harvested areas, whereas
 359 the performances of pDSSAT-emulator and CARAIB-emulator were relatively worse.



360
 361 **Figure 4** Correlation coefficient (R) and mean absolute error (MAE) over current cropland in the baseline
 362 (C360T0W0N200). As the ORCHIDEE-crop has not simulated yield under C360T0W0N200
 363 perturbation, we used the C360T0W10N200 as the baseline. The dot denotes the median and the error
 364 bar denotes the interquartile range from all grid cells in which the crop is grown according to the
 365 SPAM2010 data.

366 3.2.3 Performance of multiple emulators ensemble at grid scale

367 The multi-emulators ensemble median was able to reproduce the year-to-year variation
 368 of gridded yield over current cropland in the baseline (C360T0W0N200) from 1981 to
 369 2010. The temporal correlation coefficient R between GCM simulated and emulated
 370 yield time series over most current harvested areas were greater than 0.80.7 (multi-
 371 model ensemble median) (**Figure 5**), and the uncertainty (standard deviation) of R across
 372 emulators was smaller than 0.20.3 (Figure [S3S1](#)). The mean absolute error (MAE) and
 373 mean relative error (MRE) over most current harvested areas were mostly smaller than
 374 1 t/a and 1030%, respectively (Figure [S4S2](#)). The spatial pattern of MRE for four crops
 375 all showed a hotspot of large MRE in the Middle East, and for maize the hotspot of
 376 great MRE was also found in the southern China (Figure [S4S2](#)).



377

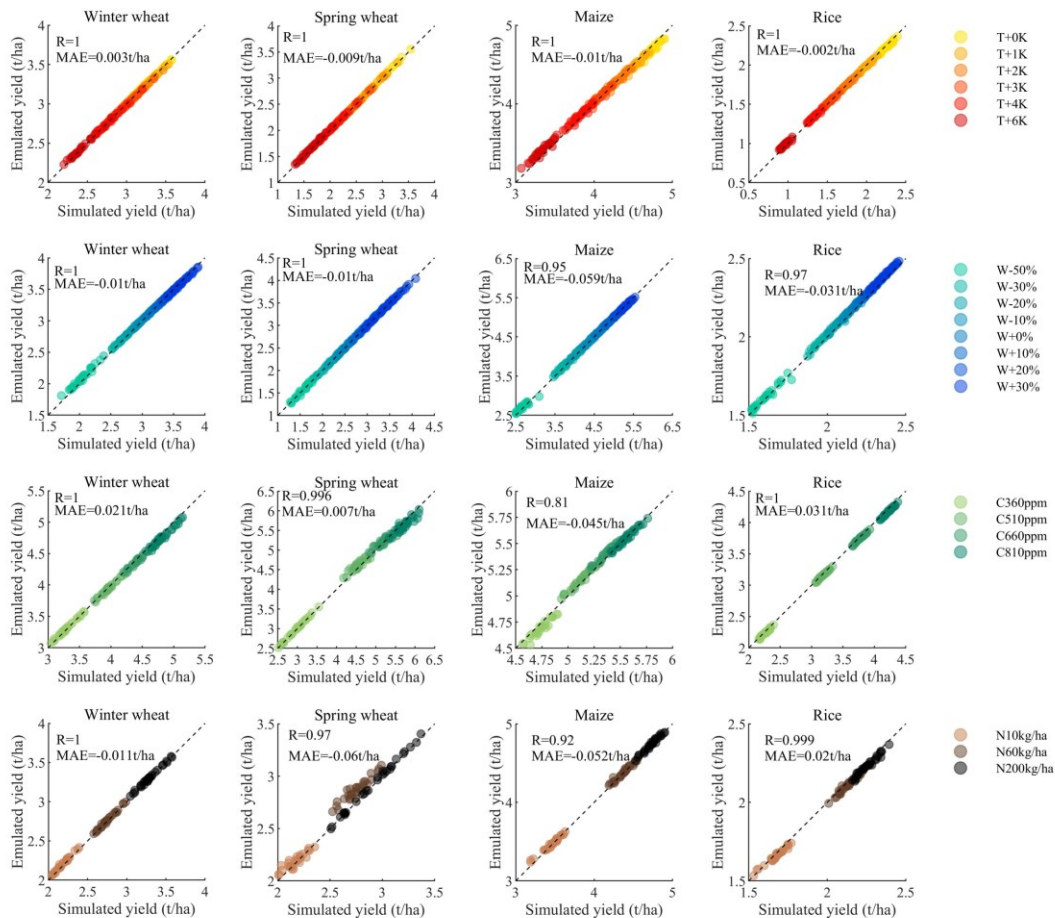
378 **Figure 5** Multi-model ensemble median R in the baseline over current cropland. R : correlation coefficient
 379 between simulated and emulated yield time series of each GGCM from 1981 to 2010.

380 **3.3 Performance of emulators to capture the year-to-year variation of GGCM**
 381 **yield in the CTWN cube**

382 **3.3.1 Performance of individual emulators at the global scale**

383 The agreement of year-to-year variation of global average yield between simulation and
 384 emulation was consistent with changes in CTWN cube over present cropland (**Figure**
 385 **6**). Under varied CTWN perturbations, the emulator could well reproduce the year-to-
 386 year variation of global mean yield from 1981 to 2010. Even when the temperature
 387 perturbation reached +6K, the emulator was still able to capture the year-to-year
 388 variation of global mean yield. Similarly, when the precipitation was less than baseline
 389 by 50%, the year-to-year variation of emulated global mean yield was well matched
 390 with those of GGCM simulation. Additionally, the fertilizations of elevated CO₂
 391 concentration and nitrogen application have been well reproduced by emulator. Similar
 392 capacity in reproducing the annual global mean yield was also been found in other
 393 emulators ([Figure S5](#) [Table S1](#) & [Table S2](#)). Even under the concurrent warm and
 394 drought condition, i.e. T+6K and W-50%, the year-to-year variation of global mean

395 yield could be well reproduced by emulator (Figure S63).



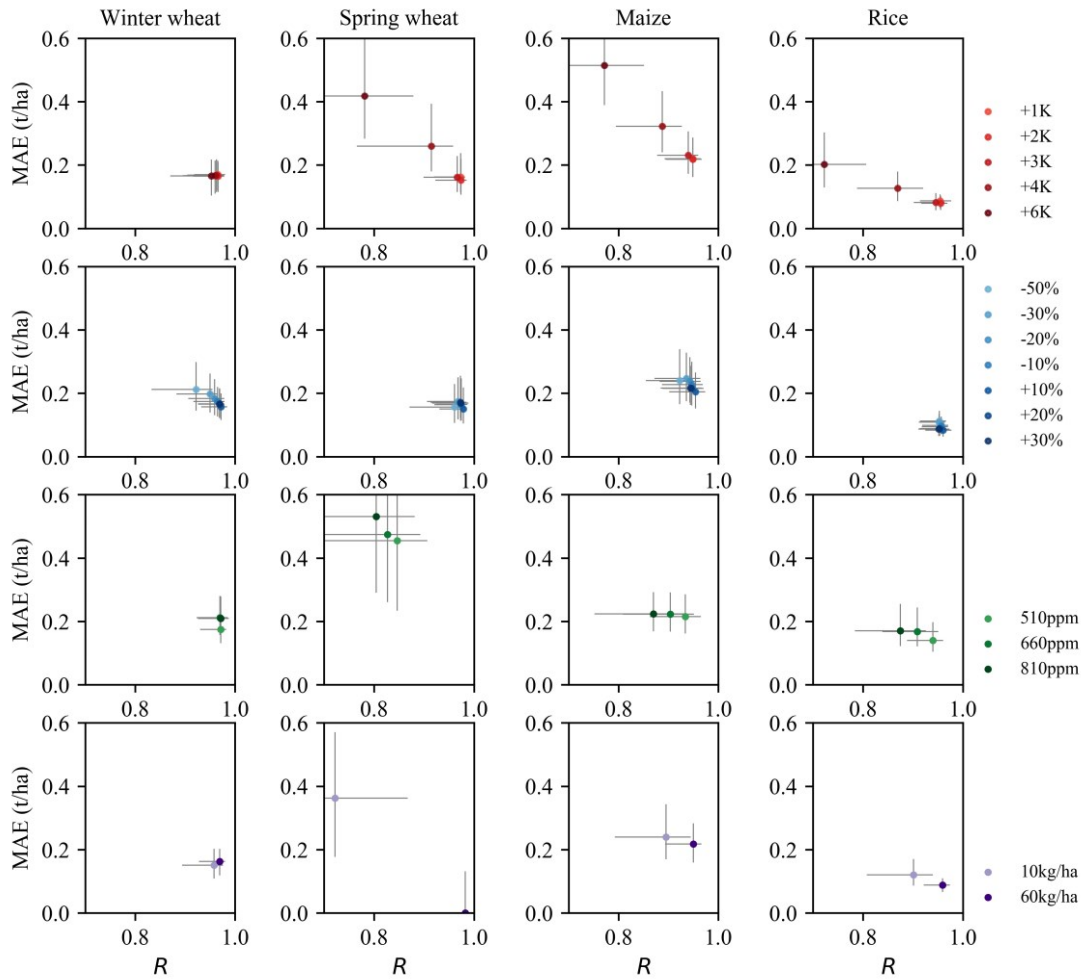
396

397 **Figure 6** Performance of one exemplary emulator (LPJmL-A0) in reproducing the year to year variation
 398 of global mean yield from 1981 to 2010 under varied individual CTWN perturbations. Each point with
 399 the same color is yield in one year. The performances of other emulators are similar to LPJmL-A0, which
 400 can be referred in the [Figure S5 for EPIC TAMU Table S1 and Table S2](#).

401 3.3.2 Performance of individual emulators at the grid scale under single 402 perturbation

403 To illustrate the performance of individual emulators to reproduce annual yield
 404 variation, we selected the LPJmL-A0 emulator as an example. The R-MAE scatter plots
 405 of LPJmL-A0 illustrated the response of gridded accuracy to varied perturbations of
 406 CTWN (**Figure 7**). The changes in accuracy of emulators under single CTWN
 407 perturbations were small with largest differences in spring wheat for modifications in
 408 the CO₂ (C) and nitrogen (N) dimensions, ~~and for rice for modifications in the water~~
 409 ~~(W) dimension~~. The overall accuracy could be kept on the high level, with greater R

410 and smaller MAE. Under temperature perturbations, the median R_s of emulators for
411 four crops were greater than 0.90.7, and the range of R_s was smaller than 0.030.2. The
412 median MAEs of emulators for four crops were less than 0.350.55, and the variation of
413 median MAEs was smaller than 0.020.2 from +1 to +6K perturbations. For precipitation
414 perturbations, the median R_s of emulators for four crops were greater than 0.880.85,
415 meanwhile the difference of median R_s across varied precipitation perturbations was
416 smaller than 0.060.1. The median MAEs of emulators for four crops was smaller than
417 0.380.3, and the range of median MAEs variation was as small as 0.050.06. The median
418 R_s and MAEs of emulators for four crops under CO₂ concentration perturbations and
419 nitrogen perturbations were comparable to those under temperature and precipitation
420 perturbations, except for spring wheat. Although the performance of spring wheat
421 emulator under CO₂ and nitrogen perturbations was not as good as other crops, the
422 median R_s was still greater than 0.75 and the median MAEs were smaller than 0.20.6.
423 Similar pattern of other emulators' performances under single perturbations at grid scale
424 are shown in the Table S2-S1 and Table S3S2.



425

426 **Figure 7** *R*-MAE scatter of the exemplary emulator (LPJmL-A0) under varied single CTWN
 427 perturbations. Each dot denotes the median of *R* or MAE over current cropland, the error bar denotes the
 428 interquartile range. *R*: correlation coefficient, MAE: mean absolute error. More details of other emulators
 429 can refer to Table S21 and S32.

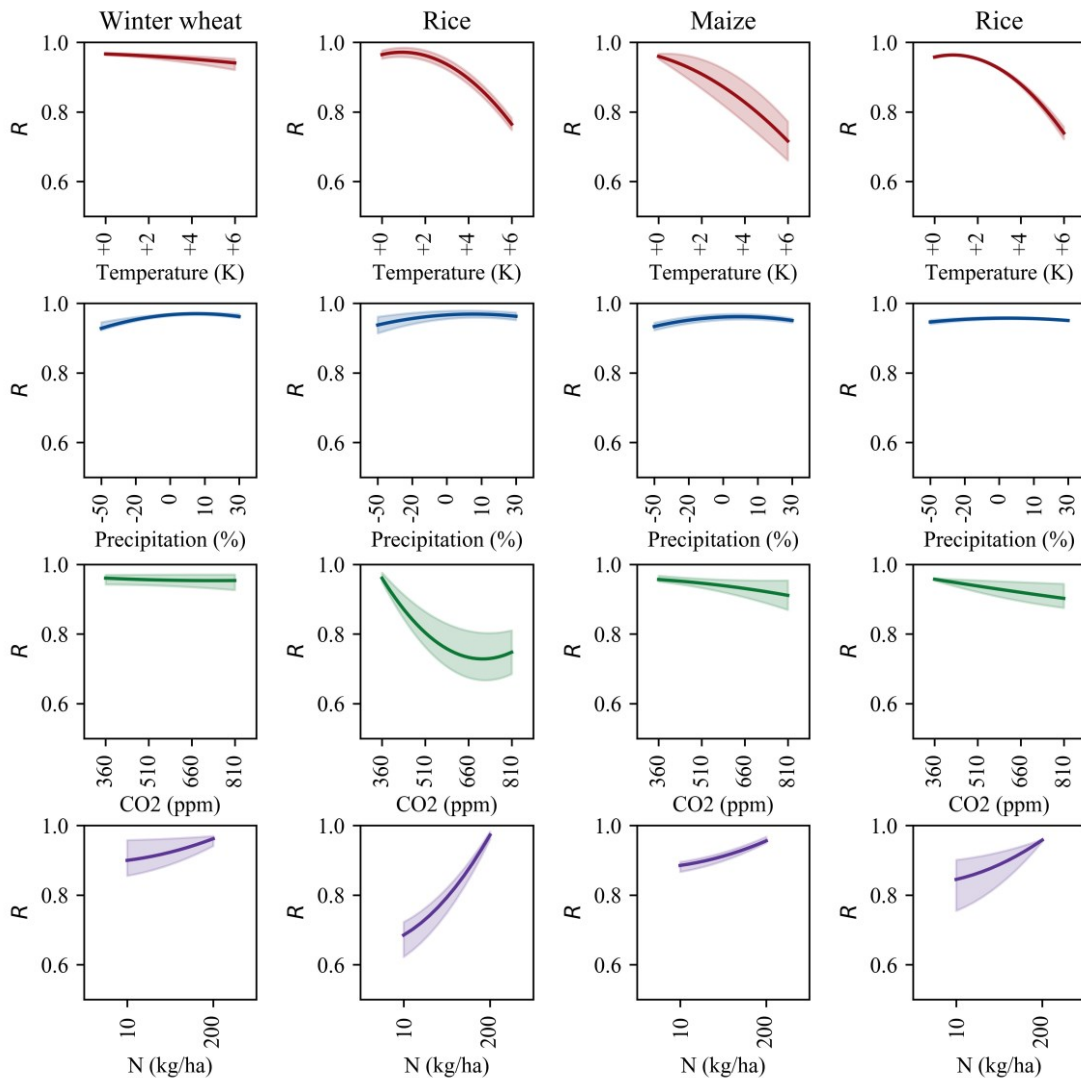
430 3.3.3 Performance of multiple emulators ensemble at the grid scale under single 431 perturbation

432 When looking at the ensemble of multiple emulators, the *R*s and MAEs under CTWN
 433 cubes was not divergent obviously (**Figure 8, Figure 9**).

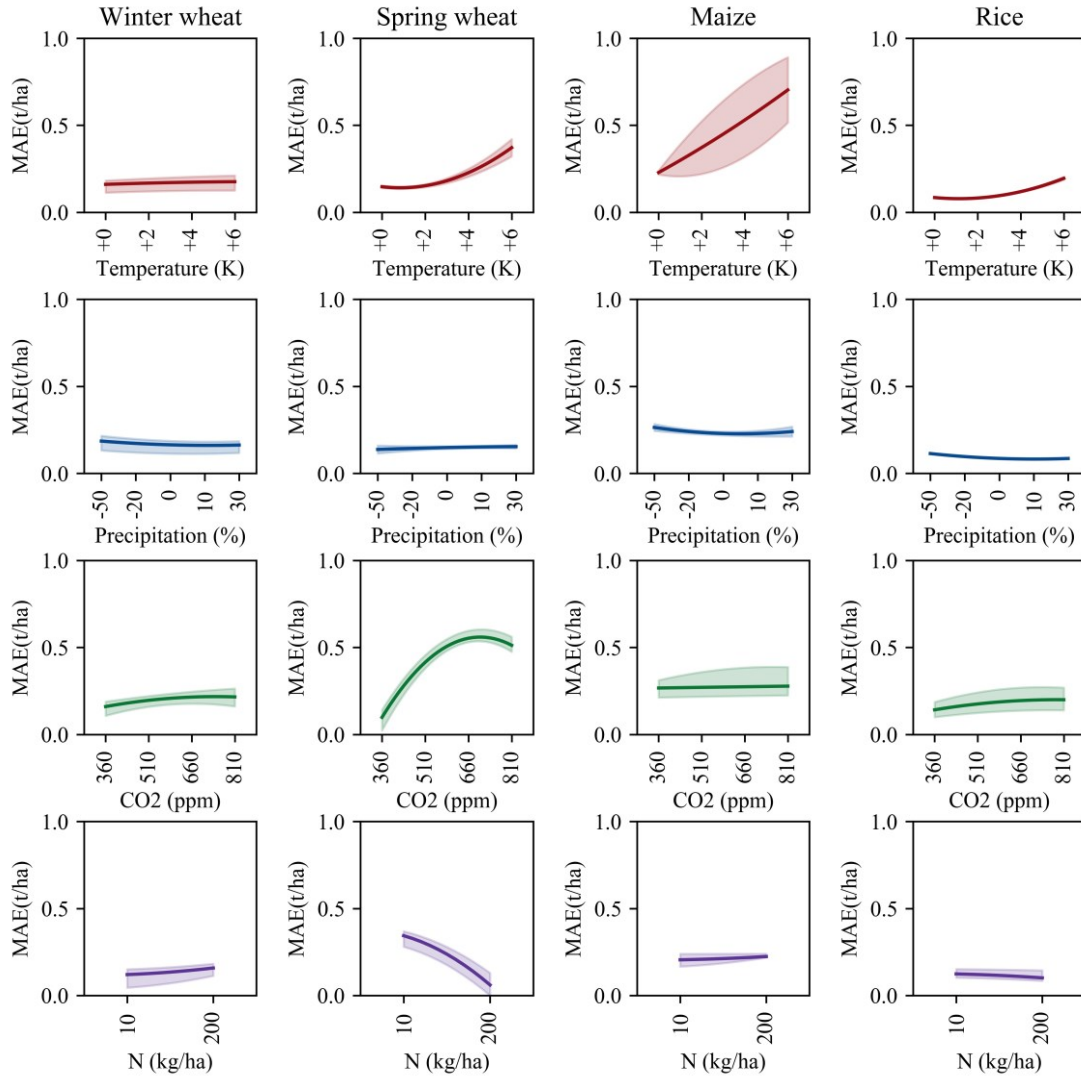
434

435 Under temperature perturbations, the range of model-ensemble median *R*s across
 436 multiple emulators was smaller than 0.010.2, and the range of median MAEs was as
 437 small as 0.030.4t/ha. For precipitation perturbation, the difference in median *R*s was
 438 less than 0.03, and the changes in median MAEs was less than 0.090.1t/ha. Under the

439 perturbation of CO₂ concentration, the emulators for winter wheat, maize and rice
 440 showed a greater median *R*s which ranged from 0.960.89 to 0.98. The variation of
 441 median MAEs was smaller than 0.080.09t/ha. The median *R*s of emulator for spring
 442 wheat, however, tended to decline under 810ppm perturbation substantially and the
 443 median MAEs tended to increase simultaneously. Similarly, for nitrogen perturbation,
 444 the range of median *R*s was less than 0.150.27, and the range of median MAEs was
 445 smaller than 0.10.3t/ha, except for emulators of spring wheat and rice. The declined *R*
 446 and increased MAE were caused by the reduction of valid sample size from the GGCM
 447 output yield under CO₂ and nitrogen perturbations (Figure S47 & Figure S58).



448
 449 **Figure 8** Correlation coefficient (*R*) of multiple emulators ensemble under varied TW perturbations. The
 450 line denotes the median of *R* over current cropland, and the shaded area denotes the range of median *R*
 451 over current cropland across emulators.



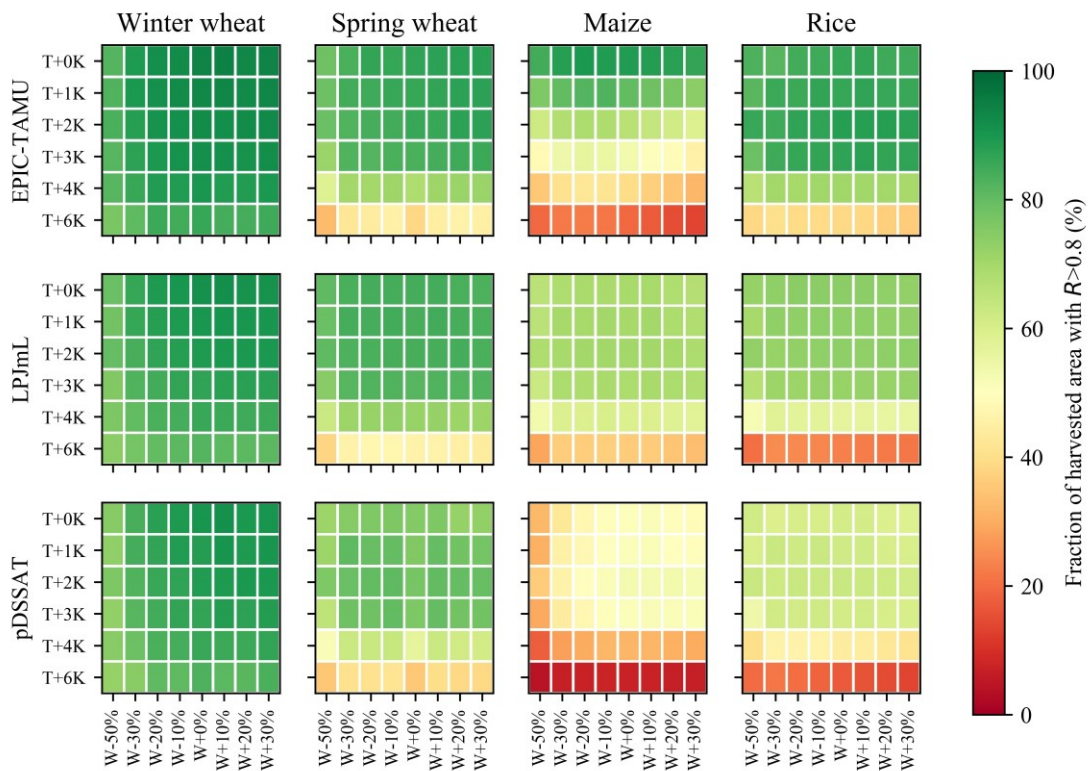
452

453 **Figure 9** Mean absolute error (MAE) of multiple emulators ensemble under varied CTWN
 454 perturbations. The line denotes the median of R over current cropland, and the shaded area denotes
 455 the range of median R over current cropland across emulators.

456 3.3.4 Performance of multiple emulators at grid scale under dual perturbations

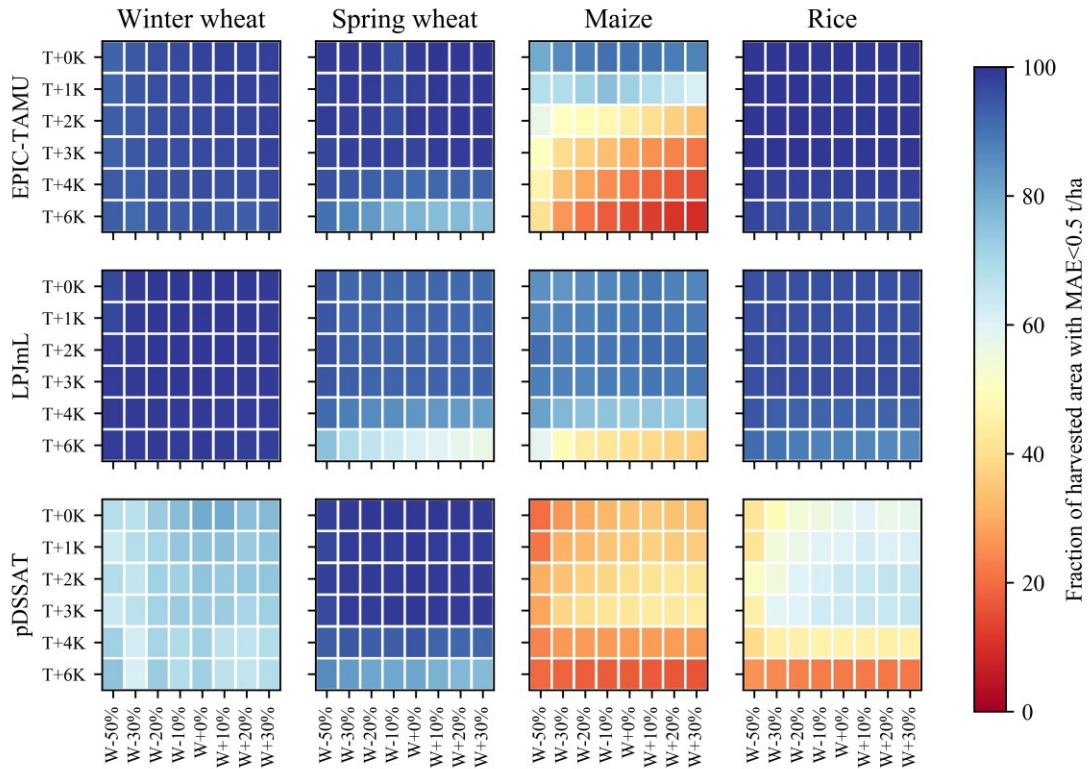
457 The performance of emulators was influenced by changes in simultaneous perturbations
 458 in two different CTWN dimensions (dual perturbations). The emulators performed well
 459 over most of current cropland but at extreme increases in T and reductions in W (**Figure**
 460 **10**), the emulators could represent the GGCM-simulated year-to-year variation only
 461 on substantially smaller shares of the current cropland. The fraction of current areas
 462 with R greater than 0.8 was the highest in the baseline but decreases under warmer and
 463 drier conditions. The fraction reduced to less than ~~60~~40% under compound T+6K and

464 W-50% perturbation, which illustrated the poor capacity of emulator under compound
 465 hot-dry conditions. However, the fraction of harvested areas with MAE smaller than
 466 0.5 t/ha did not vary much across T+W perturbations (**Figure 11**). The performance of
 467 emulators under dual perturbations for wheat were better than those for maize and rice.
 468 The fraction of maize and rice harvested area with R greater than 0.8 was relatively
 469 smaller than that of wheat. The maize harvested area with MAE smaller than 0.5 t/ha
 470 was smaller than other crops. Among the three GGCMs with full range of CTWN
 471 perturbations, the fraction of harvested area with high accuracy for LPJmL-emulator
 472 and pDSSAT-emulator was more than EPIC-TAMU-emulator.



473

474 **Figure 10** Fraction of harvested areas with high correlation coefficient ($R > 0.8$) under varied T+W
 475 perturbations. Example of EPIC-TAMU-A0, LPJmL-A0 and pDSSAT-A0 emulator because only these
 476 three GGCMs contain full range of CTWN perturbations for all four crops.



477

478 **Figure 11** Fraction of harvested areas with low mean absolute error (MAE<0.5 t/ha) under varied T+W
 479 perturbations. Example of EPIC-TAMU-A0, LPJmL-A0 and pDSSAT-A0 emulator because these three
 480 GCGMs contain full range of CTWN perturbations for all four crops.

481 4. Discussion

482 4.1 Emulator trained to capture year-to-year variation in crop yield

483 Our emulator was designed to reproduce the year-to-year variation of crop yield.
 484 Therefore, the annual yield was the target variable in emulator fitting. To capture the
 485 year-to-year crop yield variation well, the climatic predictors were divided into growing
 486 season average, daily variation and climatic extremes to capture the possible drivers of
 487 yield variation. The predictors engineering referred to the existing knowledges
 488 compiled into crop models that year-to-year variation of crop yield is associated with
 489 growing season temperature and precipitation (Ray et al., 2015), extreme heat (Iizumi
 490 and Ramankutty, 2016) and drought (Heinicke et al., 2022). The temperature and
 491 precipitation have been confirmed to be the dominant drivers to crop yield variability

492 (Schauberger et al., 2016). Moreover, the interaction between soil type and climate was
493 considered in our emulator design. Although CO₂ concentration and soil type were not
494 regarded as important contributors to yield variability, their interaction with climate
495 could also influence the yield variability (Kadam et al., 2014). The role of soil type has
496 been uncovered by previous emulator fitted by multivariate regression that the average
497 effect of temperature and precipitation differed greatly depending on soil type (Blanc,
498 2017). Compared with the emulator designed to reproduce the climatological mean
499 yield, our emulator is more suitable to project the changes in yield variability (Liu et
500 al., 2021b).

501

502 We developed the emulators with one statistical relationship for each crop between
503 GGCM simulated yield and predictors for all grids over global lands. Each grid cell
504 represents a sample in the soil-climate-fertilizer continuum, and the training data have
505 no lateral relationships. However, the response of simulated crop yield to climate
506 change was spatially heterogeneous, which mainly depends on the cultivars. Therefore,
507 one statistical relationship between yield and climatic predictors was hard to be fully
508 appropriate for each grid. In response, we used the length of growing season, a
509 representative predictor of cultivar characteristics, to adjust the global statistical
510 relationship to each grid. Therefore, predictors contained both temporal varied and
511 constant variables. The temporal varied predictors were climatic variables which
512 mainly played the role in reproduce the annual yield variation, and the temporal
513 constant predictors were non-climatic variables, like growing season length, delineated
514 the spatial distinction of crop yield response to climate. Compared with region-specific
515 emulator development, combining the temporal varied and constant predictors was
516 more concise and could profit from a broader range of data in the training set.

517 **4.2 Potential application of the well performed emulators in related fields**

518 The good performance over most grid cells indicated the potential capacity of emulators
519 in spatiotemporal downscaling, projecting annual yield in the future and multi-model

520 ensemble simulation.

521

522 The emulator could be used to conduct spatiotemporal yield downscaling because the
523 good performance of individual emulator in reproducing the annual crop yield variation
524 in the baseline. As the emulator in this study was developed with a regression-based
525 machine learning technique by using all the grid-year data points, the emulation is not
526 limited to the spatial resolution of the training data. The emulator can be applied to any
527 point with information on the predictors and can produce yield projections is as finely
528 resolved as the forcing input. From the aspect of time series of yield, the raw GGCM
529 data includes empty values (“NaN”) in some year-grid cell data points, which may be
530 caused by the lack of regional data for calibration. The vacancy of yield time series in
531 some grids could be imputed by the emulator (Folberth et al., 2019), similar to studies
532 which generated spatiotemporal continuous gridded crop yield data (Chen et al., 2022;
533 Iizumi et al., 2014).

534

535 The emulator was able to project the annual yield in the future climate scenarios, which
536 depends on the individual emulator performed well in reproducing annual yield under
537 CTWN cubes. In contrast to many previous emulators developed with historical crop
538 model simulations (Xu et al., 2021), our emulator could reproduce the CO₂ fertilization
539 effect which is an important forcing in future. The recently developed emulator based
540 on GGCM phase2 simulation under CTWN cubes could only project the
541 climatological-mean yield because the target variable in emulation was the
542 climatological-mean yield (Franke et al., 2020a). In contrast, our emulator can project
543 the annual yield variation and is not constrained by the maximum warming considered
544 in the GGCM phase2 data set (T+6K), but by the maximum temperature within the
545 training data set (warmest grid cell +6K), so that the applicability is broader (Müller et
546 al., 2021).

547

548 It is more efficient to conduct multi-model ensemble simulation with emulators than

549 GGCMs, as the emulators show good skill in reproducing GGCMs' results and the
550 emulators drastically reduce the computational time and memory requirement and
551 expertise to operate process-based crop models. First, the input of multiple emulators
552 was consistent and compatible but the inputs of raw GGCM were divergent and
553 incompatible because the structure of input data and file format of each GGCM was
554 designed independently. Second, the time-scale of emulator input was monthly or
555 growing seasonal, which was less complex than daily inputs of GGCMs. Apart from
556 the ensemble simulation, the multiple emulators could also be used to explore and
557 disentangle the uncertainty across models.

558 **4.3 Uncertainties**

559 The weaknesses of machine learning algorithm and raw GGCM have brought some
560 uncertainties into the emulators. The uncertainties induced by the machine learning
561 algorithm was as follows:

562

563 (1) When the climate factors went beyond the range of training data, the weakness of
564 machine learning in out-of-sample prediction could bring great uncertainty. The
565 emulator inputs should be capped by the range of training data. The limit of our
566 emulator was the warmest grid under +6K perturbation. As there is polar amplification,
567 the strongest warming mostly happens in cooler regions. Thus, the projected
568 temperature exceeding training range would not be widespread over global croplands.

569

570 ~~(2) The random selection of testing samples in machine learning algorithm failed to~~
571 ~~warrant independence from training samples when dependence structure exist in the~~
572 ~~data (Meyer and Pebesma, 2021; Ploton et al., 2020). In our cross-validation, the~~
573 ~~adjusted R^2 s were likely to be overestimated when using the 10-fold cross-validation~~
574 ~~approach with randomly selected trained and validated samples due to the spatial~~
575 ~~autocorrelated simulated yield. By using the leave one out validation approach, the~~
576 ~~overestimation of adjusted R^2 s has been reduced after excluding the spatial~~

577 ~~autocorrelation. Yet, the emulators derived from the 10-fold cross validation and leave-~~
578 ~~one-out validation approach are not directly comparable in terms of goodness-of-fit~~
579 ~~statistics due to completely different parameters trained. We then carefully compared~~
580 ~~the relative feature importance. As shown in Figure S9-S12, relative importance of~~
581 ~~predictors was consistent across the two validation strategies. That said, the emulator~~
582 ~~trained and validated by 10-fold cross validation with randomly selected samples can~~
583 ~~reproduce the climate yield relationship similar to that derived from the leave one out~~
584 ~~validation approach, in spite of over-estimation of the goodness-of-fit statistics. In~~
585 ~~model application, we would suggest use the emulators derived from the 10-fold cross~~
586 ~~validation due to its random sampling to avoid any potential biased estimation. But~~
587 ~~users still should be cautious when describing the accuracy of the machine learning~~
588 ~~based emulators. Still, model goodness-of-fits were reasonably good for emulating.~~
589 ~~Considering the spatial autocorrelation when fitting a machine learning model could~~
590 ~~provide a more objective understanding of model accuracy.~~

591
592 (23) Although the emulators could reproduce the GGCM annual yield with high
593 accuracy in most cases, there were cases that the machine learning algorithm did not
594 show good reproduction skill. As the emulated function intended to smooth the
595 response of simulated crop yield to climate, samples at the margins of training data tend
596 to show lower emulator skill. The extreme conditions, i.e. +6K, -50% water, 810ppm,
597 10kgN/ha, show reduced R and increased MAE. Using the emulators to estimate annual
598 crop yield under extreme perturbation conditions should be conducted with caution and
599 the additional uncertainty induced by the emulators should be considered in the
600 interpretation of results.

601
602 (34) Last but not the least, as the emulators are intended as lightweight tools that could
603 replicate the raw GGCMs, their capability in simulating crop yields is limited to the
604 capability of the original GGCMs. This raises the issue that emulators are unlikely to
605 show good performance in simulating crop yield responses to climate extremes, exactly

606 like the raw GGCMs, which have shown poor performance in capturing the yield
607 impact of heatwave and drought (Heinicke et al., 2022), and the lack of negative effect
608 of excessive wetness (Li et al., 2019a). Resolving such a problem requires the
609 improvement of raw GGCMs' capability in simulating yield response to climate
610 extremes, or statistical promotion of the GGCMs' outputs under extreme weather events.

611 **5. Conclusion**

612 In this study, we developed the machine-learning based statistical crop yield emulators
613 to reproduce the year-to-year variation of crop yield to perturbations in CO₂
614 concentration, temperature, water and nitrogen-application rate from the GGCM phase
615 2 archives. To examine the potential value of these emulators, we evaluated the
616 performance of emulators at global and gridded scale under baseline, under single and
617 dual perturbations.

618

619 The results indicated that the performance of emulators was good enough to reproduce
620 the year-to-year variation of global average crop yield in the baseline ($R > 0.98$), and
621 the difference of accuracy between individual GGCM emulators were not large.
622 Similarly, under single and dual perturbations, the capacity of emulators in reproducing
623 the year-to-year variation of global mean crop yield was not substantially changed. At
624 gridded level, the performance of emulators over most of the current croplands in the
625 baseline was still good in the sense that R was greater than 0.80.6 and MAE was smaller
626 than 0.51 t/ha. The performance of individual emulators was consistently good under
627 single CTWN perturbations, without substantial changes in R and MAE. Similarly, the
628 multiple emulators also performed well in reproducing the annual yield under single
629 CTWN perturbations, and the most grid cells across the current cropland showed
630 greater R and smaller MAE under simultaneous perturbations of T and W. The overall
631 good capacity of emulators in reproducing the year-to-year variation of GGCM
632 simulated crop yield indicated the role of emulators in spatiotemporal downscaling,

633 crop yield projection and multi-model ensemble simulation. The emulators were able
634 to boost the ability to assess crop yield failure risk under future climate change and help
635 to better understand food stability and climate risk adaptation.
636

637 **Code availability**

638 The python function for crop model emulators are available at
639 <https://doi.org/10.5281/zenodo.7796686>

640 **Author contributions**

641 WL and TY designed the research. WL, TY and CM prepared the manuscript. All
642 authors contributed to editing the manuscript.

643 **Competing interests**

644 Some authors are members of the editorial board of GMD. The peer-review process
645 was guided by an independent editor, and the authors have also no other competing
646 interests to declare.

647 **Acknowledgment**

648 This study was supported by State Key Laboratory of Earth Surface Processes and
649 Resource Ecology of China (2022-ZD-06), the National Natural Science Foundation of
650 China (42171075).
651

652 **References**

- 653 Blanc, E. and Sultan, B.: Emulating maize yields from global gridded crop models using statistical
654 estimates, *Agric. For. Meteorol.*, 214–215, 134–147, doi:10.1016/j.agrformet.2015.08.256, 2015.
- 655 Blanc, É.: Statistical emulators of maize, rice, soybean and wheat yields from global gridded crop
656 models, *Agric. For. Meteorol.*, 236, 145–161, doi:10.1016/j.agrformet.2016.12.022, 2017.
- 657 Blanc, É.: Statistical emulators of irrigated crop yields and irrigation water requirements, *Agric. For.*
658 *Meteorol.*, 284(January), 107828, doi:10.1016/j.agrformet.2019.107828, 2020.
- 659 Campbell, B. M., Vermeulen, S. J., Girvetz, E., Loboguerrero, A. M. and Ramirez-Villegas, J.:
660 Reducing risks to food security from climate change, *Glob. Food Sec.*, 11, 34–43,
661 doi:10.1016/j.gfs.2016.06.002, 2016.
- 662 Chen, S., Liu, W., Feng, P., Ye, T., Ma, Y. and Zhang, Z.: Improving Spatial Disaggregation of Crop
663 Yield by Incorporating Machine Learning with Multisource Data: A Case Study of Chinese Maize
664 Yield, *Remote Sens.*, 14(10), doi:10.3390/rs14102340, 2022.
- 665 Chen, T. and Guestrin, C.: XGBoost: A Scalable Tree Boosting System, in *Proceedings of the 22Nd*
666 *ACM SIGKDD International Conference on Knowledge Discovery and Data Mining*, pp. 785–
667 794, ACM, New York, NY, USA., 2016.
- 668 Elliott, J., Müller, C., Deryng, D., Chryssanthacopoulos, J., Boote, K. J., Büchner, M., Foster, I.,
669 Glotter, M., Heinke, J., Iizumi, T., Izaurralde, R. C., Mueller, N. D., Ray, D. K., Rosenzweig, C.,
670 Ruane, A. C. and Sheffield, J.: The Global Gridded Crop Model Intercomparison: data and
671 modeling protocols for Phase 1 (v1.0), *Geosci. Model Dev.*, 8(2), 261–277, doi:10.5194/gmd-8-
672 261-2015, 2015.
- 673 Folberth, C., Baklanov, A., Balkovič, J., Skalský, R., Khabarov, N. and Obersteiner, M.: Spatio-
674 temporal downscaling of gridded crop model yield estimates based on machine learning, *Agric.*
675 *For. Meteorol.*, 264(May 2018), 1–15, doi:10.1016/j.agrformet.2018.09.021, 2019.
- 676 Franke, J. A., Müller, C., Elliott, J., Ruane, A. C., Jägermeyr, J., Balkovic, J., Ciais, P., Dury, M.,
677 Falloon, P. D., Folberth, C., François, L., Hank, T., Hoffmann, M., Izaurralde, R. C., Jacquemin,
678 I., Jones, C., Khabarov, N., Koch, M., Li, M., Liu, W., Olin, S., Phillips, M., Pugh, T. A. M.,
679 Reddy, A., Wang, X., Williams, K., Zabel, F. and Moyer, E. J.: The GGCM Phase 2 emulator:
680 Global gridded crop model response to changes in CO₂, temperature, water, and nitrogen
681 (protocol version 1.0), *Geosci. Model Dev.*, 13(5), 2315–2336, doi:10.5194/gmd-13-2315-2020,
682 2020a.
- 683 Franke, J. A., Müller, C., Elliott, J., Ruane, A. C., Jägermeyr, J., Balkovic, J., Ciais, P., Dury, M.,
684 Falloon, P. D., Folberth, C., François, L., Hank, T., Hoffmann, M., Izaurralde, R. C., Jacquemin,
685 I., Jones, C., Khabarov, N., Koch, M., Li, M., Liu, W., Olin, S., Phillips, M., Pugh, T. A. M.,
686 Reddy, A., Wang, X., Williams, K., Zabel, F. and Moyer, E. J.: The GGCM Phase 2 experiment:
687 Global gridded crop model simulations under uniform changes in CO₂, temperature, water, and
688 nitrogen levels (protocol version 1.0), *Geosci. Model Dev.*, 13(5), 2315–2336, doi:10.5194/gmd-
689 13-2315-2020, 2020b.
- 690 Frieler, K., Schauburger, B., Arneth, A., Balkovič, J., Elliott, J., Folberth, C., Deryng, D., Müller, C.,
691 Olin, S., Pugh, T. A. M., Schaphoff, S., Schewe, J., Schmid, E., Warszawski, L. and Levermann,
692 A.: Understanding the weather signal in national crop-yield variability Earth ’ s Future, *Earth’s*
693 *Futur.*, 5, 605–616, doi:10.1002/ef2.217, 2017.

694 Fronzek, S., Pirttioja, N., Carter, T. R., Bindi, M., Hoffmann, H., Palosuo, T., Ruiz-Ramos, M., Tao, F.,
695 Trnka, M., Acutis, M., Asseng, S., Baranowski, P., Basso, B., Bodin, P., Buis, S., Cammarano, D.,
696 Deligios, P., Destain, M. F., Dumont, B., Ewert, F., Ferrise, R., François, L., Gaiser, T., Hlavinka,
697 P., Jacquemin, I., Kersebaum, K. C., Kollas, C., Krzyszczyk, J., Lorite, I. J., Minet, J., Minguez,
698 M. I., Montesino, M., Moriondo, M., Müller, C., Nendel, C., Öztürk, I., Perego, A., Rodríguez, A.,
699 Ruane, A. C., Ruget, F., Sanna, M., Semenov, M. A., Slawinski, C., Stratonovitch, P., Supit, I.,
700 Waha, K., Wang, E., Wu, L., Zhao, Z. and Rötter, R. P.: Classifying multi-model wheat yield
701 impact response surfaces showing sensitivity to temperature and precipitation change, *Agric.*
702 *Syst.*, 159(June 2017), 209–224, doi:10.1016/j.agry.2017.08.004, 2018.

703 Hasegawa, T., Sakurai, G., Fujimori, S., Takahashi, K., Hijioaka, Y. and Masui, T.: Extreme climate
704 events increase risk of global food insecurity and adaptation needs, *Nat. Food*, 2(8), 587–595,
705 doi:10.1038/s43016-021-00335-4, 2021.

706 Heinicke, S., Frieler, K., Jägermeyr, J. and Mengel, M.: Global gridded crop models underestimate
707 yield responses to droughts and heatwaves, *Environ. Res. Lett.*, 0–68 [online] Available from:
708 <https://iopscience.iop.org/article/10.1088/1748-9326/ac592e>, 2022.

709 Iizumi, T. and Ramankutty, N.: Changes in yield variability of major crops for 1981–2010 explained by
710 climate change, *Environ. Res. Lett.*, 11(3), 34003, doi:10.1088/1748-9326/11/3/034003, 2016.

711 Iizumi, T., Yokozawa, M., Sakurai, G., Travasso, M. I., Romanenkov, V., Oettli, P. and Newby, T.:
712 Historical changes in global yields : major cereal and legume crops from 1982 to 2006, , 346–357,
713 doi:10.1111/geb.12120, 2014.

714 Jägermeyr, J., Robock, A., Elliott, J., Muller, C., Xia, L., Khabarov, N., Folberth, C., Schmid, E., Liu,
715 W., Zabel, F., Rabin, S. S., Puma, M. J., Heslin, A., Franke, J., Foster, I., Asseng, S., Bardeen, C.
716 G., Toon, O. B. and Rosenzweig, C.: A regional nuclear conflict would compromise global food
717 security, *Proc. Natl. Acad. Sci. U. S. A.*, 117(13), 7071–7081, doi:10.1073/pnas.1919049117,
718 2020.

719 Jägermeyr, J., Müller, C., Ruane, A., Elliott, J., Balkovic, J., Castillo, O., Faye, B., Foster, I., Folberth,
720 C., Franke, J., Fuchs, K., Guarin, J., Heinke, J., Hoogenboom, G., Iizumi, T., Jain, A. ., Kelly, D.,
721 Khabarov, N., Lange, S., Lin, T., Liu, W., Mialyk, O., Minol, S. and Rosenzweig, C.: Climate
722 change signal in global agriculture emerges earlier in new generation of climate and crop models,
723 *Nat. Food* (in Revis., 2021).

724 Janssens, C., Havlík, P., Krisztin, T., Baker, J., Frank, S., Hasegawa, T., Leclère, D., Ohrel, S.,
725 Ragnauth, S., Schmid, E., Valin, H., Van Lipzig, N. and Maertens, M.: Global hunger and climate
726 change adaptation through international trade, *Nat. Clim. Chang.*, 10(9), 829–835,
727 doi:10.1038/s41558-020-0847-4, 2020.

728 Jones, J. W., Antle, J. M., Basso, B., Boote, K. J., Conant, R. T., Foster, I., Godfray, H. C. J., Herrero,
729 M., Howitt, R. E., Janssen, S., Keating, B. A., Munoz-Carpena, R., Porter, C. H., Rosenzweig, C.
730 and Wheeler, T. R.: Brief history of agricultural systems modeling, *Agric. Syst.*, 155, 240–254,
731 doi:10.1016/j.agry.2016.05.014, 2017.

732 Kadam, N. N., Xiao, G., Melgar, R. J., Bahuguna, R. N., Quinones, C., Tamilselvan, A., Prasad, P. V.
733 V and Jagadish, K. S. V: Chapter Three - Agronomic and Physiological Responses to High
734 Temperature, Drought, and Elevated CO₂ Interactions in Cereals, vol. 127, edited by D. B. T.-A.
735 in A. Sparks, pp. 111–156, Academic Press., 2014.

736 Kinnunen, P., Guillaume, J. H. A., Taka, M., D’Odorico, P., Siebert, S., Puma, M. J., Jalava, M. and
737 Kummu, M.: Local food crop production can fulfil demand for less than one-third of the

738 population, *Nat. Food*, 1(4), 229–237, doi:10.1038/s43016-020-0060-7, 2020.

739 Li, Y., Guan, K., Schnitkey, G. D., DeLucia, E. and Peng, B.: Excessive rainfall leads to maize yield
740 loss of a comparable magnitude to extreme drought in the United States, *Glob. Chang. Biol.*,
741 25(7), 2325–2337, doi:10.1111/gcb.14628, 2019a.

742 Li, Y., Guan, K., Yu, A., Peng, B., Zhao, L., Li, B. and Peng, J.: Toward building a transparent
743 statistical model for improving crop yield prediction: Modeling rainfed corn in the U.S, *F. Crop.*
744 *Res.*, 234(January), 55–65, doi:10.1016/j.fcr.2019.02.005, 2019b.

745 Liu, W., Ye, T. and Shi, P.: Decreasing wheat yield stability on the North China Plain: Relative
746 contributions from climate change in mean and variability, *Int. J. Climatol.*, 41(S1), E2820–
747 E2833, doi:10.1002/joc.6882, 2021a.

748 Liu, W., Ye, T., Jägermeyr, J., Müller, C., Chen, S., Liu, X. and Shi, P.: Future climate change
749 significantly alters interannual wheat yield variability over half of harvested areas, *Environ. Res.*
750 *Let.*, 16(9), 094045, doi:10.1088/1748-9326/ac1fbb, 2021b.

751 Liu, W., Li, Z., Li, Y., Ye, T., Chen, S. and Liu, Y.: Heterogeneous impacts of excessive wetness on
752 maize yields in China: Evidence from statistical yields and process-based crop models, *Agric. For.*
753 *Meteorol.*, 327(August), 109205, doi:10.1016/j.agrformet.2022.109205, 2022.

754 Lobell, D. B., Sibley, A. and Ivan Ortiz-Monasterio, J.: Extreme heat effects on wheat senescence in
755 India, *Nat. Clim. Chang.*, 2(3), 186–189, doi:10.1038/nclimate1356, 2012.

756 Makowski, D., Asseng, S., Ewert, F., Bassu, S., Durand, J. L., Li, T., Martre, P., Adam, M., Aggarwal,
757 P. K., Angulo, C., Baron, C., Basso, B., Bertuzzi, P., Biernath, C., Boogaard, H., Boote, K. J.,
758 Bouman, B., Bregaglio, S., Brisson, N., Buis, S., Cammarano, D., Challinor, A. J., Confalonieri,
759 R., Conijn, J. G., Corbeels, M., Deryng, D., De Sanctis, G., Doltra, J., Fumoto, T., Gaydon, D.,
760 Gayler, S., Goldberg, R., Grant, R. F., Grassini, P., Hatfield, J. L., Hasegawa, T., Heng, L., Hoek,
761 S., Hooker, J., Hunt, L. A., Ingwersen, J., Izaurralde, R. C., Jongschaap, R. E. E., Jones, J. W.,
762 Kemanian, R. A., Kersebaum, K. C., Kim, S. H., Lizaso, J., Marcaida, M., Müller, C., Nakagawa,
763 H., Naresh Kumar, S., Nendel, C., O’Leary, G. J., Olesen, J. E., Oriol, P., Osborne, T. M.,
764 Palosuo, T., Pravia, M. V., Priesack, E., Ripoche, D., Rosenzweig, C., Ruane, A. C., Ruget, F.,
765 Sau, F., Semenov, M. A., Shcherbak, I., Singh, B., Singh, U., Soo, H. K., Steduto, P., Stöckle, C.,
766 Stratonovitch, P., Streck, T., Supit, I., Tang, L., Tao, F., Teixeira, E. I., Thorburn, P., Timlin, D.,
767 Travasso, M., Rötter, R. P., Waha, K., Wallach, D., White, J. W., Wilkens, P., Williams, J. R.,
768 Wolf, J., Yin, X., Yoshida, H., Zhang, Z. and Zhu, Y.: A statistical analysis of three ensembles of
769 crop model responses to temperature and CO₂ concentration, *Agric. For. Meteorol.*, 214–215,
770 483–493, doi:10.1016/j.agrformet.2015.09.013, 2015.

771 Meyer, H. and Pebesma, E.: Predicting into unknown space? Estimating the area of applicability of
772 spatial prediction models, *Methods Ecol. Evol.*, 12(9), 1620–1633, doi:10.1111/2041-
773 210X.13650, 2021.

774 Mistry, M. N., Sue Wing, I. and De Cian, E.: Simulated vs. empirical weather responsiveness of crop
775 yields: US evidence and implications for the agricultural impacts of climate change, *Environ. Res.*
776 *Let.*, 12(7), doi:10.1088/1748-9326/aa788c, 2017.

777 Müller, C., Franke, J., Jägermeyr, J., Ruane, A. C., Elliott, J., Moyer, E., Heinke, J., Falloon, P.,
778 Folberth, C., Francois, L., Hank, T., Izaurralde, R. C., Jacquemin, I., Liu, W., Olin, S., Pugh, T.,
779 Williams, K. E. and Zabel, F.: Exploring uncertainties in global crop yield projections in a large
780 ensemble of crop models and CMIP5 and CMIP6 climate scenarios, *Environ. Res. Let.*,
781 doi:10.1088/1748-9326/abd8fc, 2021.

782 Nachtergaele, F., Velthuizen, H. Van, Verelst, L., Batjes, N., Dijkshoorn, K., Engelen, V. Van, Fischer,
 783 G., Jones, A., Montanarella, L., Petri, M., Prieler, S., Teixeira, E., Wiberg, D. and Shi, X.:
 784 Harmonized World Soil Database (version 1), *Soil Sci.*, p.38, doi:3123, 2009.
 785 Ostberg, S., Schewe, J., Childers, K. and Frieler, K.: Changes in crop yields and their variability at
 786 different levels of global warming, *Earth Syst. Dyn.*, 9(2), 479–496, doi:10.5194/esd-9-479-2018,
 787 2018.
 788 Pirttioja, N., Carter, T. R., Fronzek, S., Bindi, M., Hoffmann, H., Palosuo, T., Ruiz-Ramos, M., Tao, F.,
 789 Trnka, M., Acutis, M., Asseng, S., Baranowski, P., Basso, B., Bodin, P., Buis, S., Cammarano, D.,
 790 Deligios, P., Destain, M. F., Dumont, B., Ewert, F., Ferrise, R., François, L., Gaiser, T., Hlavinka,
 791 P., Jacquemin, I., Kersebaum, K. C., Kollas, C., Krzyszczak, J., Lorite, I. J., Minet, J., Minguez,
 792 M. I., Montesino, M., Moriondo, M., Müller, C., Nendel, C., Öztürk, I., Perego, A., Rodríguez, A.,
 793 Ruane, A. C., Ruget, F., Sanna, M., Semenov, M. A., Slawinski, C., Stratonovitch, P., Supit, I.,
 794 Waha, K., Wang, E., Wu, L., Zhao, Z. and Rötter, R. P.: Temperature and precipitation effects on
 795 wheat yield across a European transect: A crop model ensemble analysis using impact response
 796 surfaces, *Clim. Res.*, 65, 87–105, doi:10.3354/cr01322, 2015.
 797 Ploton, P., Mortier, F., Réjou-Méchain, M., Barbier, N., Picard, N., Rossi, V., Dormann, C., Cornu, G.,
 798 Viennois, G., Bayol, N., Lyapustin, A., Gourlet-Fleury, S. and Pélissier, R.: Spatial validation
 799 reveals poor predictive performance of large-scale ecological mapping models, *Nat. Commun.*,
 800 11(1), 1–11, doi:10.1038/s41467-020-18321-y, 2020.
 801 Portmann, F. T., Siebert, S. and Döll, P.: MIRCA2000—Global monthly irrigated and rainfed crop
 802 areas around the year 2000: A new high-resolution data set for agricultural and hydrological
 803 modeling, *Global Biogeochem. Cycles*, 24(1), doi:10.1029/2008GB003435, 2010.
 804 Raimondo, M., Nazzaro, C., Marotta, G. and Caracciolo, F.: Land degradation and climate change:
 805 Global impact on wheat yields, *L. Degrad. Dev.*, 32(1), 387–398, doi:10.1002/ldr.3699, 2021.
 806 Ray, D. K., Gerber, J. S., Macdonald, G. K. and West, P. C.: Climate variation explains a third of
 807 global crop yield variability, *Nat. Commun.*, 6, 1–9, doi:10.1038/ncomms6989, 2015.
 808 Ruane, A. C., Goldberg, R. and Chryssanthacopoulos, J.: Climate forcing datasets for agricultural
 809 modeling: Merged products for gap-filling and historical climate series estimation, *Agric. For.*
 810 *Meteorol.*, 200, 233–248, doi:10.1016/j.agrformet.2014.09.016, 2015.
 811 Sacks, W. J., Deryng, D., Foley, J. A. and Ramankutty, N.: Crop planting dates: an analysis of global
 812 patterns, *Glob. Ecol. Biogeogr.*, 19(5), 607–620, doi:10.1111/j.1466-8238.2010.00551.x, 2010.
 813 Schauburger, B., Rolinski, S. and Müller, C.: A network-based approach for semi-quantitative
 814 knowledge mining and its application to yield variability, *Environ. Res. Lett.*, 11(12),
 815 doi:10.1088/1748-9326/11/12/123001, 2016.
 816 Shahhosseini, M., Martinez-Feria, R. A., Hu, G. and Archontoulis, S. V.: Maize yield and nitrate loss
 817 prediction with machine learning algorithms, *Environ. Res. Lett.*, 14(12), 124026,
 818 doi:10.1088/1748-9326/ab5268, 2019.
 819 Sternberg, T.: Regional drought has a global impact, *Nature*, 472(7342), 169–169,
 820 doi:10.1038/472169d, 2011.
 821 Tartarini, S., Vesely, F., Movedi, E., Radegonda, L., Pietrasanta, A., Recchi, G. and Confalonieri, R.:
 822 Biophysical models and meta-modelling to reduce the basis risk in index-based insurance: A case
 823 study on winter cereals in Italy, *Agric. For. Meteorol.*, 300, 108320,
 824 doi:https://doi.org/10.1016/j.agrformet.2021.108320, 2021.
 825 Troy, T. J., Kipgen, C. and Pal, I.: The impact of climate extremes and irrigation on US crop yields,

826 Environ. Res. Lett., 10(5), 1–10, doi:10.1088/1748-9326/10/5/054013, 2015.
827 Xu, H., Zhang, X., Ye, Z., Jiang, L., Qiu, X., Tian, Y., Zhu, Y. and Cao, W.: Machine learning
828 approaches can reduce environmental data requirements for regional yield potential simulation,
829 Eur. J. Agron., 129(August 2020), doi:10.1016/j.eja.2021.126335, 2021.
830 Zhu, X. and Troy, T. J.: Agriculturally Relevant Climate Extremes and Their Trends in the World's
831 Major Growing Regions, Earth's Futur., 6(4), 656–672, doi:10.1002/2017EF000687, 2018.
832